Study of Carbon Black-Epoxy based Fat Tissue Phantom and its Dielectric Properties

HATEM MOHAMED ABDELWAHAB AL-GABROUN

DISSERTATION SUBMITTED IN FULFILMENT
OF THE REQUIREMENTS
FOR THE DEGREE OF MASTER OF SCIENCE ENGINEERING

FACULTY OF ENGINEERING
UNIVERSITY OF MALAYA
KUALA LUMPUR

2010

UNIVERSITI MALAYA ORGINAL LITERARY WORK DECLARATION

Name of candidate: **HATEM M.ALGABROUN** I.C. Passport No: 991894

Registration/Matric No: **KGA060001**

Name of Degree: **Master**

Title of Thesis: **STUDY OF CARBON BLACK-EPOXY BASED FAT TISSUE PHANTOM AND ITS DIELECTRIC PROPERTIES**

Field of study: **Biomedical Engineering**

I do solemnly and sincerely declare that:

(1) I am the sole author/writer of this work;
(2) This work is original;
(3) Any use of any work in which copyright exists was done by way of fair dealing and for permitted purposes and any excerpt or extract form, or reference to or reproduction of any copyright work has been disclosed expressly and sufficiently and the title of the work and its authorship have been acknowledged in this work;
(4) I do not have any actual knowledge nor do I ought reasonably to know that the making of this work constitutes an infringement of any copyright work;
(5) I hereby assign all and every rights in the copyright to this work to the University of Malaya ("UM"), who henceforth shall be owner of the copyright in this work and that any reproduction or use in any form or by any means whatsoever is prohibited without the written consent of UM having been first had and obtained;
(6) I am fully aware that if in the course of making this work I have infringed any copyright whether intentionally or otherwise, I may be subject to legal action or any other action as may be determined by UM.

Candidate's Signature: Date: 04/10/2010

Subscribed and solemnly declared before.

Witness's Signature Date: 1/10/2010

Name : Assoc Prof Dr Wahab Bin Mohd Ibrahim

Designation: Supervisor

Preface

This thesis is divided into six chapters. Chapter 1 gives background about the area of designing the biological phantoms. The objectives and method of the research were reviewed briefly. The thesis structure is presented in Chapter 1. Also problem statements were figured out. Chapter 2 presents the review and commentary of literature relevant to biological phantoms. Topics reviewed including general information about the follows:

1. Over view on microwave imaging techniques for breast cancer detection
2. Dielectric properties of human tissues at high frequencies
3. Materials have been used to simulate the dielectric properties of human tissues at microwave frequency range 1 GHz to10 GHz
4. Review on the mixing formula that used to predict the dielectric properties of mixtures
5. Attempts to predict the dielectric properties of Epoxy- Carbon Black mixtures

Chapter 3 is the methodology chapter. It shows the theoretical parts and the experimental procedures. In Chapter 4, the experimental results are presented. Then comparisons between the theoretical and experimental results are explained and discussed. The results are concluded in Chapter 5 and a number of suggestions of future works are pointed out from these conclusions.

Acknowledgements

First, I thank "GOD" for inspiring me with the strength, patience and willingness to perform this work.

I would like to convey my deepest gratitude and appreciation to my supervisor Prof. Madya Dr. W Mohd Azhar bin Wan Ibrahim from the Biomedical Engineering Department, university of Malaya, for his wisdom, patience, precious advice, guidance, encouragement and continuous valuable scientific suggestion throughout the preparation of my project. His extremely understanding and support has made the project progress smoothly.

I would like to give my best regards and acknowledgements to Prof. Dr David Smith from Northumbria University who helped me by his invaluable knowledge in this work.

I would like to thank University of Malaya - Research Unit, for funding my research.

Finally, I would like to thank my parents and all of my family for supporting, encouraging and assisting me throughout the course of my study.

Abstract

Microwave imaging techniques for medical applications have been reported in the literature for many years. However, the progress in imaging algorithms, numerical techniques, microwave hardware and computational speed has renewed the interest in this field.

Breast cancer detection is particularly attractive from a microwave imaging perspective, the major reason referred to the potentially high dielectric contrast between cancerous tissues and normal breast tissues depending on water content. Low water tissues tend to be low permittivity as fat, whilst high water content tissues tend to be high permittivity as cancerous tissues.

All of that increased the need for effective phantoms that mimic the electromagnetic properties of biological tissues at these high frequencies in a purpose of testing the mutual effects between these radiations and biological tissues. For this purpose several phantoms with several materials have been proposed to simulate biological tissues.

This study investigates a simulation method based on rule of mixture to design fat phantom by using binary system containing epoxy as a matrix and carbon black powder as a filler. The dielectric properties were measured by using Network Analyzer equipped with coaxial cable and the results showed the possibility of using this system for fat tissues simulating at frequency range from 1 GHz to 10 GHz.

Abbreviations

CB	Carbon Black
CMI	Confocal Microwave Imaging
CTT	Computed Thermo-acoustic Tomography
ECal	Electronic Calibration model
FDTD	Finite Difference Time-Domain
HWCT	High Water Content Tissues
LWCT	Low Water Content Tissues
MAP	Maximum- A-Posteriori
MIST	Microwave Imaging via Space Time
MUT	Material Under Test
NA	Network Analyzer
SAR	Specific Absorption Rate
STT	Scanning Thermo-acoustic Tomography
TSAR	Tissue Sensing Adaptive Radar
UWB	Ultra Wide-Band

Table of Contents

Declaration Page ii

Preface iii

Acknowledgements iv

Abstract v

Abbreviations vi

List of Figures x

List of Tables xii

CHAPTER 1

BACKGROUND 1

1.1 Introduction 1

1.2 Problem statement 2

1.3 Aim of study 3

1.4 Objectives of the study 3

CHAPTER 2

LITERATURE REVIEW 5

2.1 Introduction 5

2.2 Microwave imaging for breast cancer detection 5

2.2.1 Passive microwave imaging technique: 7

2.2.2 Hybrid microwave imaging techniques: 8

2.2.2.1 Computed Thermo-acoustic Tomography (CTT) 8

2.2.2.2 Scanning Thermo-acoustic Tomography (STT) 9

2.2.3 Active microwave imaging technique 9

2.2.3.1 Tomographic imaging 10

2.2.3.2 Radar system 10

2.3 Phantoms 15
2.3.1 Introduction 15
2.3.2 Dielectric properties of tissues 17
2.3.3 Tissues –equivalent phantom 18
2.3.3.1 HWCT phantoms 18
2.3.3.2 LWCT phantoms 21
2.3.3.3 Materials used for simulating HWCT & LWCT: 24
2.4 Permittivity mixing equations of heterogeneous systems 25
2.4.1 Introduction 25
2.4.2 Permittivity of heterogeneous mixtures 25
2.4.3 Epoxy - carbon black mixtures predictions at microwave frequencies of 1 GHz to 10 GHz 27
2.5 Dielectric properties measurements 31
2.5.1 Transmission/reflection line technique 32
2.5.2 Open ended coaxial probe technique 33
2.5.3 Free space technique 34
2.5.4 Resonant technique 36
CHAPTER 3
METHODOLOGY 38
3.1 Introduction 38
3.2 Materials and equipments 40
3.3 Sample preparation 41
3.4 Data collection 45
3.5 Comparison between the theoretical and the practical results 49
CHAPTER 4
RESULTS & DISCUSSIONS 51
4.1 Introduction 51

4.2 Sample measurements results of permittivity and conductivity 52
4.3 Statistical analysis of the practical results 55
4.3.1 Permittivity by frequency 55
4.3.2 Conductivity by frequency 57
4.3.3 Permittivity by concentration 58
4.3.4 Conductivity by concentration 60
4.4 Discussion of the measurement results of permittivity and conductivity 60
4.5 Comparison between theoretical and practical results of the permittivty and conductivity 62
4.6 Statistical analysis for the practical and theortical results of permittivity and conductivity 64
4.7 Discussion of the comparison between the theoretical and practical results of the permittivty and conductivity 66
4.8 Comparison between the modified equation and the practical results of the permittivity and conductivity 67
4.9 Statistical analysis for the practical and theoretical (after modification) results of permittivity and conductivity at frequency range 1 GHz to10 GHz 69
4.10 Discussion of the comparison between the modified equation and the practical results of the permittivity and conductivity 71

CHPTER 5

CONCLUSION & FUTURE WORK 73
5.1 Conclusion 73
5.2 Future work 74

REFERENCES 75

APPENDIX 81

List of Figures

Figure 2.1 The Microwave Imaging Techniques for Breast Cancer Detection 6

Figure 2.2 a) Passive technique, b) Hybrid technique, c) Active technique [13] 7

Figure 2.3 The received signals are shown in the central panel. When the beamformer is steered to location r_0 (the actual location of a scatterer), the signals added coherently, as shown in the left justified. When the beamformer is steered to a location other than r_0, the signals added incoherently [22] 12

Figure 2.4 Microwave holographic imaging experimental setup in the University of Malaya 14

Figure 2.5 The comparison of the frequency spectrums of the dielectric constants of Carbon black/epoxy composites from experimental values and simulated results of eq.(9) 30

Figure 2.6 The comparison of the carbon black concentration dependency of the electrical conductivities of carbon black/epoxy composites from experimental values and simulated results of eq.(9) 30

Figure 2.7 Dielectric properties measurements using transmission/reflection line technique [72] 33

Figure 2.8 Dielectric properties measurements using open-ended coaxial probe technique [72] 34

Figure 2.9 Dielectric properties measurements using free space technique [65] 35

Figure 2.10 Dielectric properties measurements by using resonant cavity technique [66] . 37

Figure 3.1. Flow chart for project methodology 39

Figure 3.2 The mixing of the epoxy and CB 44

Figure 3.3 Prepared samples after smoothing and shaping for the dielectric properties measurements 44

Figure 3.4 The used equipments for the dielectric properties measurements. 45

Figure 3.5 The NA calibration using distilled water at room temperature. 47

Figure 3.6 Block diagram in general of the dielectric properties measurements 48

Figure 3.7 The dielectric properties measurements in progress 49

Figure 4.1 Permittivity measurements at frequency (1-10) GHz 53

Figure 4.2 Conductivity measurements at frequency (1-10) GHz 53

Figure 4.3 Permittivity with various concentrations at selected frequency.....54

Figure 4.4 Conductivity with various concentrations at selected frequency.....54

Figure 4.5 Permittivity comparisons between Prac and Theo at the 7 concentration values (levels of concentration "P") and at frequency (1-10) GHz..... 63

Figure 4.6 Conductivity comparisons between Prac and Theo at the 7 concentration values (levels of concentration "P") and at frequency (1-10) GHz..... 63

Figure 4.7 Permittivity comparisons between Prac and Theo (after the modification) at the 7 concentration values (levels of concentration "P") at frequency (1-10) GHz 68

Figure 4.8 Conductivity comparisons between Prac and Theo (after the modification) at the 7 concentration values (levels of concentration "P") at frequency (1-10) GHz 68

List of Tables

Table 2.1 Comparison between the measurement techniques [65] 32

Table 3.1 Carbon black (XE2) specifications 40

Table 3.2 Epoxy (BONDITE 8950-1A/B) specifications 40

Table 3.3 Volume fraction of components in samples 43

Table 4.1 Levene's Test of Equality of Error Variances of the permittivity by frequency .. 56

Table 4.2 Tukey's post hoc test of the permittivity by frequency 56

Table 4.3 One-way ANOVA analysis of permittivity by frequency 57

Table 4.4 Levene's Test of Equality of Error Variances of the conductivity by frequency. 57

Table 4.5 One-way ANOVA analysis of conductivity by frequency 58

Table 4.6 Levene's Test of Equality of Error Variances of the permittivity by concentration 58

Table 4.7 Tukey's post hoc test of the permittivity by concentration 59

Table 4.8 One-way ANOVA analysis of permittivity by concentration 59

Table 4.9 One-way ANOVA analysis of conductivity by concentration 60

Table 4.10 Permittivity Paired Samples Test of Prac-Theo 64

Table 4.11 Permittivity Paired Samples Test of Prac-Theo 65

Table 4.12 Conductivity Paired Samples Test of Prac- Theo 65

Table 4.13 Conductivity Paired Samples Test of Prac- Theo 66

Table 4.14 Permittivity Paired Samples Test of Prac-Theo 69

Table 4.15 Permittivity Paired Samples Test of Prac-Theo 70

Table 4.16 Conductivity Paired Samples Test of Prac- Theo 70

Table 4.17 Conductivity Paired Samples Test of Prac- Theo 71

CHAPTER 1

BACKGROUND

1.1 Introduction

In the past few decades, studying the interaction of electromagnetic radiation and its effect on the biological tissues has been growing; since biological tissues are sometimes accidentally exposed to electromagnetic sources, such as radars, microwave ovens, etc. Also, there has been an increase in the use of electromagnetic energy in the medical field, for diagnostic purposes or therapies, as well as in the rapid expansion of mobile phone usage and other devices that emit electromagnetic energy at microwave frequencies. All of this has increased the need for effective phantoms that mimic the electromagnetic properties of biological tissues at high frequencies. The purpose is to test the mutual effects between microwave radiations and biological tissues [1].

A phantom is a physical model made from tissue-equivalent materials which imitate the characteristics of biological tissue and wave distribution inside the human body [2, 3]. Human tissues roughly tend to fall into one of two groups i.e. low water content, and high water content. Since human tissues vary considerably depending on the water content, low water tissues such as bone and fat tend to have low permittivity, whilst high water content tissues as muscle, and internal organs, tend to have high permittivity [1, 2, 4]. Therefore, it is possible to divide phantoms into two groups depending on the simulated tissues, namely, High Water Content Tissues phantom (HWCT) and Low Water Content Tissues phantom (LWCT) [5].

This research focuses on designing a LWCT phantom to be used as fat tissue for microwave imaging applications. There have been several successful recipes for making LWCT phantoms [2,3]. However, most of the LWCT phantoms suffer from certain disadvantages such as high cost, instability over time, complex making procedure and hard shaping. Furthermore, it seems that all the previous phantoms are based on trial and error to be made; there are no equations that can be used to predict or to adjust the dielectric properties of the phantom. This research is aiming to design a phantom that overcomes all the above problems of LWCT, by using mixing equations.

1.2 Problem Statement

In the past few decades, the interest in designing phantoms that imitate the dielectric properties of biological tissues at high frequencies has been growing, since biological tissues may often accidentally exposed to electromagnetic sources such as radars, microwave ovens, mobile phones, etc; or purposely such as in medical field. One such emerging medical application is Microwave Breast Cancer Imaging, which is currently under research in the University of Malaya and many other parts of the world [1, 5].

However, the designed phantom to exhibit similar dielectric properties should be equivalent in both parts of the complex permittivity, that is, if the complex permittivity of biological medium, namely, ($\varepsilon'_b - J\,\varepsilon''_b$), is known, the corresponding phantom material should have the permittivity values $\varepsilon'_p = \varepsilon'_b$ and $\varepsilon''_p = \varepsilon''_b$ [6]. In addition, it is necessary for the phantom to be fixed in dimension, to be able to compare the obtained images with the known dimension, and to be able to investigate the precision of the system. Furthermore, the

chosen materials for designing the phantom should be very good in stability over time so the produced phantom can be used repeatedly.

This study was focusing on designing hard phantom for breast fat tissue, since it is the majority type of tissue in the breast. However, the current fat phantoms suffer from several problems such as hard shaping, instability over time, complex making procedure and high cost. In addition, there are no mixing equations that can be used to adjust the dielectric properties of the phantom.

This work concentrated on designing fat phantom by using a binary system that overcomes all the above problems.

1.3 Aim of Study

The aim of this study was to develop a hard phantom using a binary system that imitates the dielectric properties of the breast fat tissues at frequencies between 1 GHz to 10 GHz by utilizing a mixing formula that predicts the dielectric properties of the resultant phantom.

1.4 Objectives of the Study

The objectives of this study were to design a hard phantom for fat breast tissues using an Epoxy- Carbon Black (CB) mixture to be used in the application of microwave breast cancer detection. For this purpose, several research objectives were lined-out to tackle the main objective of this research, as follows:

- To test the equation that predicts the dielectric properties of Epoxy-CB mixture as a function of frequency and percentage of Carbon Black.

- To manufacture Epoxy - CB samples and to measure their dielectric properties (permittivity and conductivity)of Epoxy - CB mixtures between frequencies 1 GHz to 10 GHz by using Network Analyzer
- To investigate the designing of the phantom that simulates fat tissues by using binary system (CB-Epoxy), at microwave frequency range from 1 GHz to10 GHz.
- To conduct a thorough review of theories and techniques for microwave phantom
- To improve the ability to predict the dielectric properties of binary mixtures by modifying mixture equations.
- To compare the dielectric properties of the fat phantom with the published fat tissues measurements.

CHAPTER 2

LITERATURE REVIEW

2.1 Introduction

A comprehensive review on the related topic to this study is presented in this chapter. It starts with a review on the methods and the techniques used in microwave imaging for breast cancer detection. After a brief review on the dielectric properties of the human tissues, a comprehensive literature review on tissue equivalent phantoms is viewed. Then, mixing rules to predict the dielectric properties of heterogeneous mixtures is presented. Finally, techniques of dielectric properties measurements by using network analyzer are reviewed.

2.2 Microwave Imaging for Breast Cancer Detection

Microwave imaging techniques for medical applications have been reported in the literature for many years. However, the progress in imaging algorithms, numerical techniques, microwave hardware and computational speed has renewed interest in this field.

Larsen and Jacobi in the late 1970s started the opening of microwave imaging in biomedical applications with a development of water-immersed antenna for biomedical applications, where some images was formed of the internal structure of a Canine kidney [7]. After that, major interests have been focused on microwave imaging in biomedical applications.

Recently a major focus is applied on the breast tumor detection application using microwave imaging. Breast imaging is particularly attractive from a microwave

perspective, because of the potentially high dielectric contrast between cancerous tissues and normal breast tissues [8-12]. In addition, the breast tissue is more translucent to microwaves than many other tissues, such as muscles or brain, makes imaging several centimeters into the breast is not anticipated to be problematic [8].

Researchers have investigated different approaches to achieve a suitable system for breast cancer detection, which is shown in Figure 2.1. There are three main approaches used in Microwave Imaging techniques for Breast Cancer Detection. The three approaches are passive, hybrid, and active techniques [8, 9, 13], which is depicted in Figure 2.2.

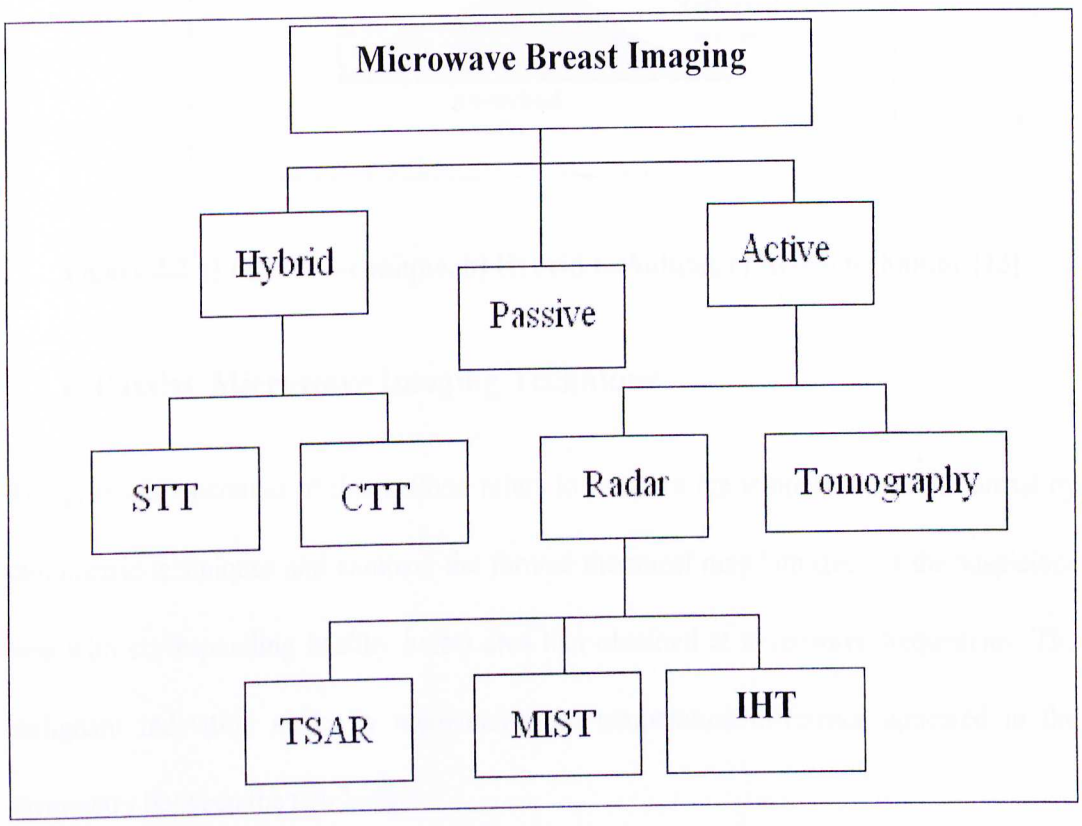

Figure 2.1 The Microwave Imaging Techniques for Breast Cancer Detection

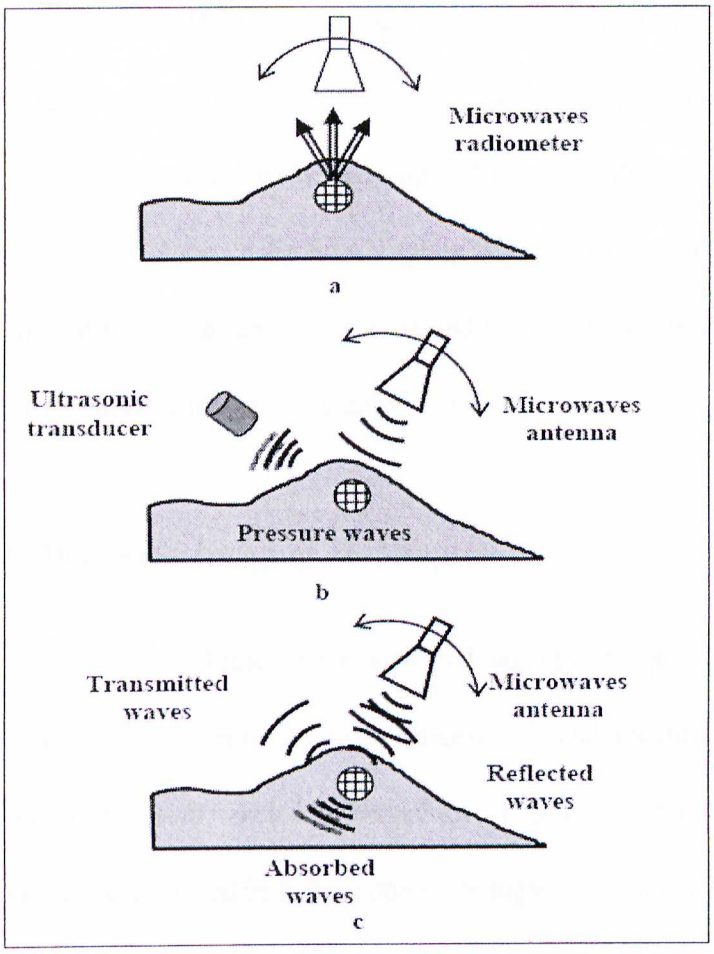

Figure 2.2 a) Passive technique, b) Hybrid technique, c) Active technique [13]

2.2.1 Passive Microwave Imaging Technique

The principle operation of this method refers to measure the temperature of the breast by radiometric techniques and compare the formed thermical map "images" of the suspicious area with corresponding healthy breast area that obtained at microwave frequencies. The malignant indication made by recognizing the temperature difference appeared in the asymmetry between the two images.

Microwave radiometry (also called thermometry or thermography) has been explored for many years especially as adjuvant to mammography. The France research group is an example; they develop a microwave system by using 6 Dicke radiometer in parallel to

decrease the time acquisition. The breast was scanned the breast in 5 mm increments and the data was recorded by each of the 6 radiometers to indicate the suspicious area. The images of two breasts (right and left) were compared to obtain the region of increased temperature [14]. Another group ONCOSCAN group is another example for microwave radiometry system and it used to scan 130 patient and the results obtained demonstrate a positive predictive combined with mammography [15].

2.2.2 Hybrid Microwave Imaging Techniques:

The hybrid approach also termed microwave-acoustic imaging technique. The principle of operation is to illuminate the breast by using microwave, and measure the signal by ultrasound transducer. Since the dielectric properties of normal and tumor tissues are different, more energy is deposited in tumors due to its higher conductivity, as a result of this absorption the tumor expanding and generates pressure waves which are detected by ultrasound transducer. The measurements made at ultrasound transducers are then translated into images to indicate the tumor location. By using this technique, microwave creates a contrast to be imaged and the ultrasound provides reasonable resolution.

Two approaches of hybrid microwave-acoustic imaging technique have been proposed, namely, Computed Thermo-acoustic Tomography (CTT) and Scanning Thermo-acoustic Tomography (STT).

2.2.2.1 Computed Thermo-acoustic Tomography (CTT)

The breast is placed in water bath and illuminate with 0.5 μs pulses of 434 MHz signals using waveguide. The pulses waves are used to generate ultrasound waves in the medical

region [16-17]. Ultrasound transducers are arranged on a hemisphere recorded signals and data are recorded as the transducers configuration is rotated through 360 degrees to collect sufficient data. Filtered back projection algorithms adapted from X-ray computed tomography has been used to form the images. The clinical results have been obtained with this method demonstrate images which show internal tissues structure in the breast.

2.2.2.2 Scanning Thermo-acoustic Tomography (STT)

Wang and his colleagues have developed STT [18-21]. In this technique, the object illuminated in the GHz region, using pulses of microwave. By using focused ultrasound transducer, signals were detected. Good experiments results were obtained with various properties and thickness phantoms containing block of fat and muscles [18-19].

2.2.3 Active Microwave Imaging Technique

The basic idea in this method is to illuminate the breast with microwaves, and the detection of incident wave by employing a set of receivers located on the opposite side of the breast or by recording the reflection at the transmitter antenna. In case of tumor presence, the breast will encounter changes in electrical properties which will cause a variation in detected energy amount at the receivers and the transmitters. Images are formed using information contained in the detected energy. Active microwave imaging technique may be classified into tomographic and radar-based system [22].

2.2.3.1 Tomographic Imaging

In tomographic systems, numerous antennas located surrounding the object to be imaged, which is immersed in water, or intralipid solution, or a weak saline solution, depending on the liquid availability and suitability of electrical properties for minimizing contrast with the body. While the position of the transmitting antenna is changed, numerous antennas receive the waves transmitted through the breast, and the process is repeated to collect sufficient data. By the transmitted (incident) and the scattered (received) fields, the shape of the object and spatial distribution of the permittivity are obtained. Since the breast is heterogeneous and its boundaries are not planner, the incident waves is scattered in all directions rather than reflected in one specific direction and likely suffers multiple reflections. This poses an inverse scattering problem that is difficult to solve due to the nonlinear relationship between the measured scattered fields and pattern (image) of the permittivity [10].

Several approaches to tomographic imaging have been proposed [23-26]. However, this method still suffering from the need to use sophisticated algorithms to form maps of the electrical property distributions in the breast. The majority of such algorithms mainly to match measurements of the microwaves scattered by the breast to results computed with a model. The presence of tumors alters the scattered signal, resulting in areas of increased permittivity and conductivity on images [10].

2.2.3.2 Radar System

The radar system was proposed for medical applications as a means to detect malignancy in internal biological breast tissues [27]. The radar-based approaches have much in common

with ground penetrating radar systems for object detection, as both methods involve detecting an anomaly in a heterogeneous background [10]. The transmitted electromagnetic waves penetrate into a region under inspection and are scattered by targets that exhibit a mismatch in dielectric properties. These scattered signals are recorded by one or more receiving antennas, and then used to infer the existence of the location of the subsurface target [22].

In contrast with the tomography method, this system does not form a map of the complete electrical properties distributions, but only identifies regions of strong scattering due to a small region of different permittivity [9, 22]. This is because malignant tumors have a larger microwave scattering cross-section than normal breast tissue heterogeneity of comparable size at the microwave frequencies. Therefore, it would be possible to pinpoint the tumors.

Although the radar system provides less detailed information about the breast, it avoids nonlinear inverse scattering techniques to simpler imaging algorithms [8]. Radar approaches use an Ultra Wide-Band pulse (UWB) for satisfying the resolution requirement. Resolution of 1cm or less in breast tissue (assuming $\varepsilon_r' = 9$) requires bandwidth of several GHz. Tissue conductivity increases with increasing frequency, so the upper frequency of the bandwidth is thus limited to approximately 10 GHz in order to provide adequate penetration into the tissue [8, 10]. Ultra-wideband frequency content is between 1 GHz and 10 GHz to regime balances between the conflicting demands of spatial resolution (better at higher frequencies) and penetration depth (better at lower frequencies) [8-10, 22]. To obtain the data, the breast is illuminated with an ultra-wideband pulse, and the reflection recorded at the same antenna. This process is repeated at a number of locations surrounding the

breast. The reflections observed at the collection of sensor locations are focused to identify the presence and the location of the tumor. In the Radar-Based system, simple time shifting and summing algorithm was applied. First, the sensor is scanned at a number of locations surrounding the breast and this is accomplished by calculating the travel time between each sensor location and the selected focal point. Next, time shifting and summing is applied to the recorded reflections, and this process is repeated as the focal point is scanned through a region of interest to create an image. If a high-contrast scattering object (such as a malignant tumor) exists at the focal point, the waveforms add coherently. Clutter signals generated by the heterogeneity of normal breast tissue surrounding the focal point will add incoherently. In this manner, tumor backscatter signals are enhanced while clutter signals are minimized as illustrated in Figure 2.3 [28].

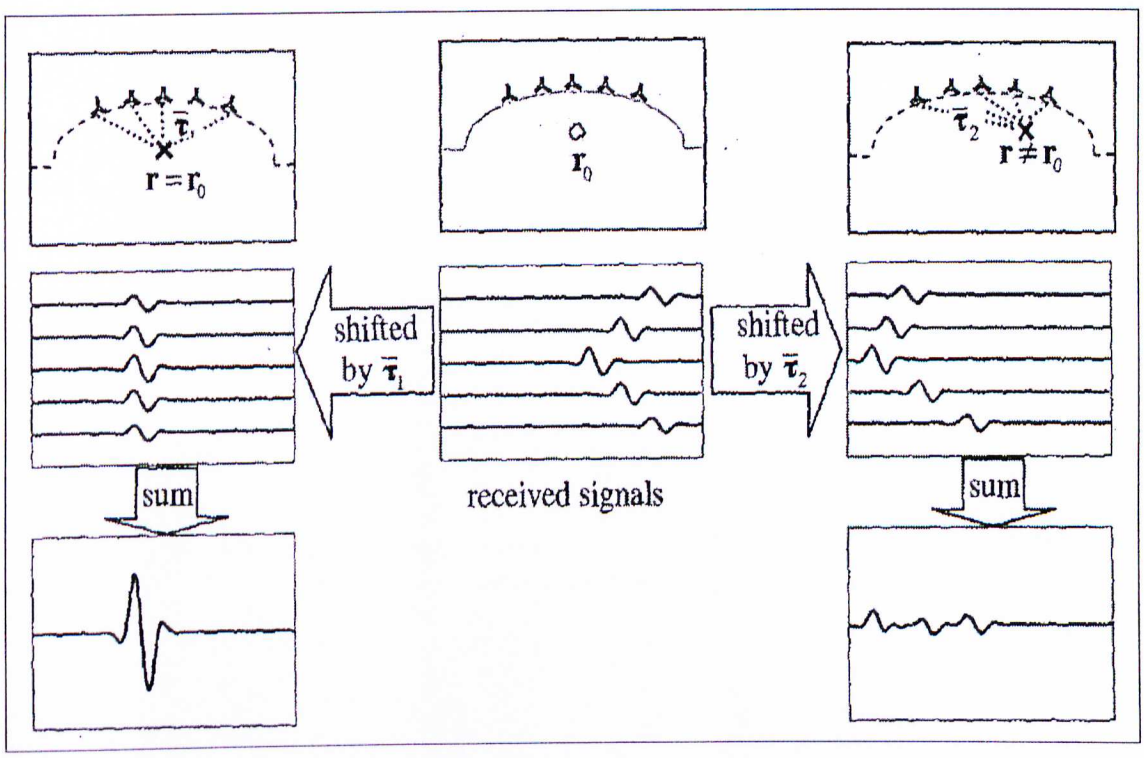

Figure 2.3 The received signals are shown in the central panel. When the beamformer is steered to location r_0 (the actual location of a scatterer), the signals added coherently, as shown in the left justified. When the beamformer is steered to a location other than r_0, the signals added incoherently [22]

There are techniques which have been investigated in the Radar-Based system [8], i.e. Microwave Imaging via Space Time (MIST), Tissue Sensing Adaptive Radar (TSAR) and Indirect Holographic Technique (IHT) [29]. Figure 2.4 demonstrates IHT found in the University of Malaya. The results of these techniques show a promising future for the Radar system [8, 29-31].

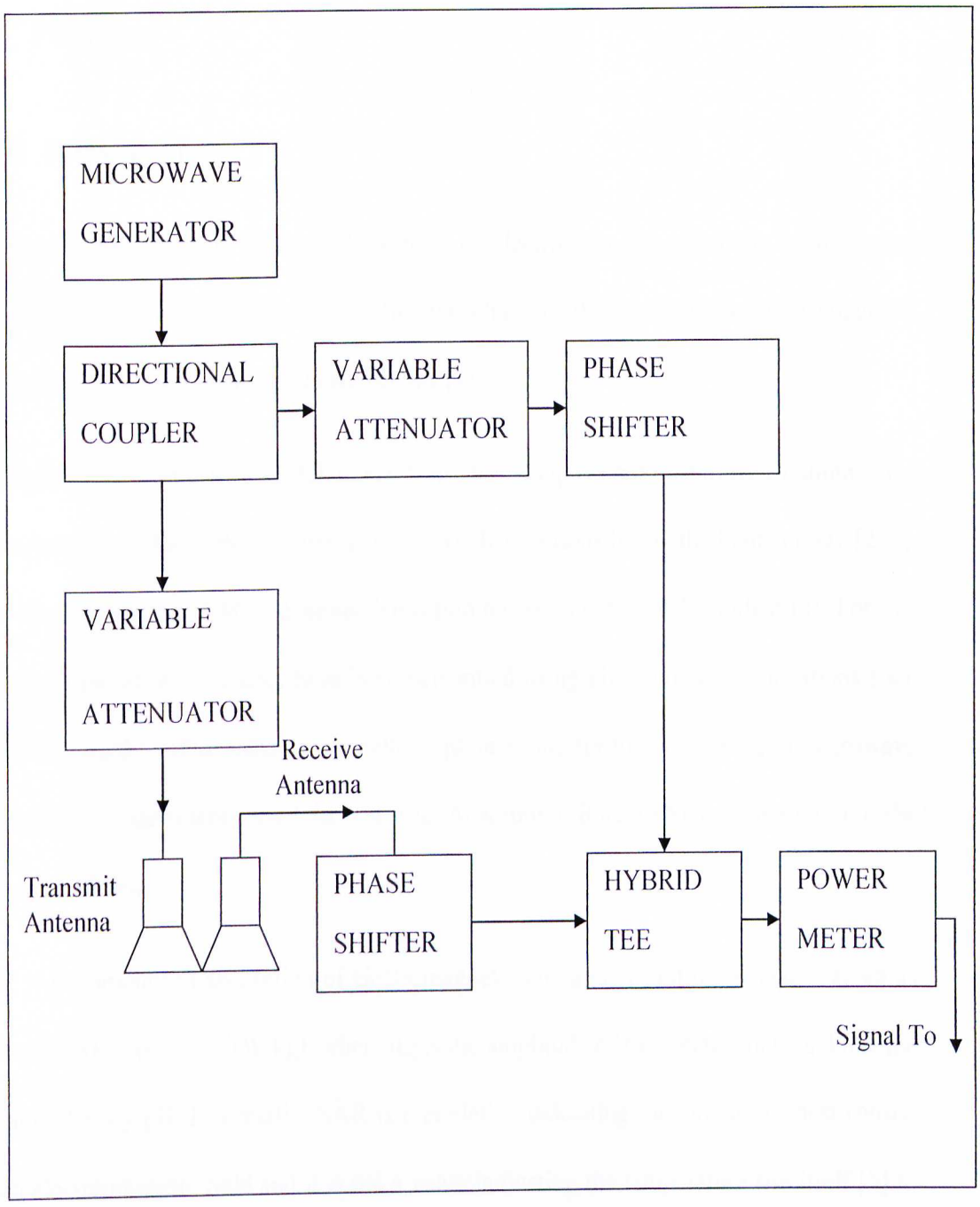

Figure 2.4 Microwave holographic imaging experimental setup in the University of Malaya

2.3 Phantoms

2.3.1 Introduction

In the past few decades, studying the effects of electromagnetic radiations on biological tissues has been growing; therefore, effective phantom that mimics the electromagnetic properties of the biological tissues are needed [1].

A phantom is a physical model made from tissue-equivalent materials to imitate the characteristics of the biological tissue and wave distributions inside the human body [2, 3]. The Electromagnetic (EM) radiations deposition has been extensively studied [4]. For this purpose some of these studies have been performed using phantoms for applications such as, estimating the safety standards of cellular phones, and for the developing of microwave hyperthermia equipments used in Specific Absorption Rate (SAR) estimation for the treatment of cancer.

SAR is the amount of absorption of electromagnetic energy per unit mass, and is given as follows, $SAR = \sigma |E|^2 / \rho$ [W/kg], where |E| is the amplitude of the electric field and ρ is the medium density [3]. Essentially, SAR is a guideline indicating the amount of heat caused by an electromagnetic field and it is not a value indicating the temperature rise itself [3].In addition, electromagnetic radiations may have hazardous effects. Safety standards (e.g. IEEE Standard C95.1 - 1999) have been defined using maximum permissible exposure to quantities, such as electric and magnetic fields, induced currents in the body. Standard C95.1-1999 indicates that acceptable devices operating between 100 kHz and 6 GHz have maximum SAR over a body of less than 1.6 W/kg when averaged over 1g of tissue. To

evaluate compliance of an EM system to the safety standard, power deposition and expected heating can be estimated with computer models [8].

Basically, various phantoms with different materials have been proposed to simulate tissues, and it is possible to classify these phantoms into three classes of equivalence between a phantom material and the corresponding biological material. They are as follows:

A) Equivalence for electrical properties of tissues, which means that the phantom material is required to have real and imaginary parts (termed complex permittivity) equal to those of the tissues to be simulated.

B) Equivalence for the internal electromagnetic power deposition, when the thermal equivalence is required besides the electrical properties, therefore, the phantom should additionally have a heating pattern corresponding to that in the simulated tissue.

C) Equivalence for the internal temperature transport, in which not only the heating pattern but also the perfusion of the temperature is simulated; however, this is very difficult to achieve [32-33].

It is well recognized that the dielectric properties of tissue are a strong function of frequency, therefore suitable phantom with the same materials ratio for all frequencies are very difficult to achieve if not impossible. Previous knowledge on the dielectric properties of the biological tissues is essential to simulate biological tissues. In the next section, the dielectric properties of tissues will be briefly introduced. Later, various phantom materials and its limitation will be presented.

2.3.2 Dielectric Properties of Tissues

Complex permittivity, ε^* of biological tissues, describes the interaction of biological tissues with microwave frequency. It is a complex quantity that consists of two separate parameters, ε' and ε'', and is expressed as:

$$\varepsilon^* = \varepsilon' - j\varepsilon'' \quad (1)$$

Where the real part of permittivity ε' is a measure of the ability to store energy from an external electric field, while the imaginary part (loss factor) indicates the energy amount that is converted into heat and dissipated. The loss factor includes the effect of the conductivity as described below.

$$\varepsilon'' = \sigma / \varepsilon_0 \omega \quad (2)$$

Where, σ is the equivalent conductivity of the medium.

The dielectric properties of biological tissues have been the subject of research for over four decades [34]. A major comprehensive survey was made in 1996 [35-36]. These studies cover a large selection of tissues over a wide spectrum of frequencies (10 Hz - 20 GHz).The most recent study was done in 2007 by Mariya Lazebnik et.al. [37], in which the scale of the dielectric properties measurements were conducted from 0.5 to 20 GHz. All these studies show that the dielectric properties of various human tissues vary considerably depending on the water content. Jonson and Guy [38] tabulated and summarized lots of literature and studies related to the dielectric properties of the human body tissues. They reported that these tissues roughly tend to fall into one of two groups, namely, low water content tissues, and high water content tissues. Low water tissues such as bone and fat tend

to be low permittivity, whilst high water content tissues such as muscle, blood, and internal organs tend to be high permittivity [1, 2, 4]. Employing this partition, the next section will provide a review on phantoms materials that have been used in research to simulate the human body.

2.3.3 Tissues –Equivalent Phantom

Making microwave phantoms normally requires mixing different materials to be similar in their dielectric properties with the tissues to be simulated. Since it is possible to divide the body tissues into two types as described in the previous section, it is also possible to divide phantoms into two types [5]. They are: a) HWCT i.e. Phantom simulating high water content tissues, b) LWCT i.e. Phantom simulating low water content tissues.

2.3.3.1 HWCT Phantoms

The seminal simulation work for the dielectric properties of tissues was done in 1971 as reported by Guy [39]. This phantom consists of saline solution (water and sodium chloride (NaCl)), a jelling agent TX-150 widely termed as 'super stuff' and polyethylene powder. Detailed descriptions of processing techniques have been reported by Chou et al.[40], by changing the ingredients. It is possible to simulate high-water-content tissues at frequencies of 13.56 - 2450 MHz [4, 15-16]. The dielectric constant can be varied over a wide range by varying the polyethylene powder ratio, and the conductivity can be controlled by changing the salinity of the material [39]. This phantom is easy to use, easy to model, and also inexpensive to prepare [4]. It was used successfully worldwide to simulate muscles from

many research workers [3, 4, 41]. However, there are problems with preservation of this phantom, due to invasion of bacteria and separation of moisture [2-3, 41-44].

Another type of materials for simulating HWCT was first introduced by Bini et al.[32], and then subsequently adapted for microwave applications by Andreuccetti et al.[45]. The base material is Acrylamide, (C_3H_5NO) polymerized in water and salt doping is added to simulate the electric properties of various types of biological tissues. The complex permittivity for the phantom was measured at five frequencies between (0.75 – 5.50) GHz. By varying the acrylamide content it is possible to control the dielectric constant ε', and the losses ε". The required conductivity is obtained by adding the adequate salt concentration. The main advantages of this phantom is its very low optical absorbance (transparent phantom), also its self standing with no mechanical support. However, this phantom has a short life time several hours when exposed to air, or weeks when kept in airtight enclosure [32,46]. Recently this phantom was adapted by other researches [47, 48], these phantoms involved complicated fabrication methods in preparing, and the used chemical might be difficult to obtain [49].

Another type of phantoms with the transparency advantage has been introduced by Robinson et al. [33] to simulate HWCT and termed EWSG. Its composition by weight is: ethanediol 48%, water 40%, salt (NaCl) 2%, and gelatin 10% [33]. The complex permittivity was measured with an open-ended coaxial sensor connected with an automatic network analyzer, by using a numerical analysis program. Complex permittivity measurements reported at 3 frequencies (500, 1000, 2450) MHz in a room temperature, and the results showed a close agreement with the literature at 1000 MHz (ε^*=49.4 -24.4j) and by changing the proportion of the contents it would be possible to simulate muscle at

other frequencies. The resultant phantom is rigid enough to hold their shape; also it is soft to be cut by a knife. It has advantages over the popular "TX- 150", it is widely used more rigid and also it is transparent [3].

Another type of HWCT phantoms that contains Agar are also being used, especially in microwave imaging researches [46, 50-51]. These phantoms consisted of agar, sodium chloride and water. Unfortunately, the electrical properties of these phantoms are not stable over time since they dry out and decompose [2]. However, Ito et al. [3] adapted this phantom to simulate brain tissues and muscle tissues. It consists of agar, polyethylene powder, sodium chloride, TX-151 (which is known as "super stuff"), preservative, and de-ionized water. The agar prevents water from separating and makes the self-shape possibility. The relative permittivity is adjusted by varying the polyethylene powder content, while the conductivity is mainly adjusted by varying the sodium chloride concentration. The TX-151 is used to increase the viscosity [3]. Measurements of the phantom electrical properties have been made by using HP85070 permittivity probe. The results showed that the electrical properties values of brain and muscle tissues are almost realized successfully with a single composition ratio at frequencies of 300 MHz to 2.5 GHz. The stability over time has been tested for the phantom. It was tested by wrapping the phantom with a plastic film to prevent drying, and kept at room temperature under observation, for more than one month. The measurements at one month (at 3 frequencies: 430 MHz, 900 MHz and 2.45 GHz) showed that there are no significant changes in its electrical properties [3].

All the above-mentioned phantoms suffer from preservation problems over time and these problems cause a changing in the phantoms' electrical properties which resulted in wrong

experiment results. Dry phantoms have been developed by researches to solve the preservation problems [2, 33, 41-42]. These phantoms have the advantage of stability even over a very long time since no water is contained [2-3]. They are constructed in two ways. The first type is composed of ceramic powder, graphite powder and resin [41]. The use of graphite is to increase the loss tangent (τ) since the loss tangent of the ceramic is very small as reported by Tamura et al. [42]. The complex permittivity of 27 test specimens was measured using coaxial line technique as a function of frequency range of (0.5 - 5) GHz. All the measurements performed using HP8510 and the results show that a wide range of permittivity can be obtained by varying the constituent ratio [47]. However, the cutting or reshaping of this phantom is not easy due to the hard ceramic content; also, special adhesive is needed to remove the air gaps between the ceramic pieces. Furthermore, this adhesive was found difficult to use [2].

The second type of dry phantoms has been investigated by Nikawa et. al. [2]. It utilizes raw silicon rubber with two kinds of carbon fibers and curing agent. Measurements of complex permittivity have been done by using reflection method and the results showed the possibility of simulating HWCL by proper selection of carbon ratio. Since this phantom contains no water, it is superior in preservation. However, special equipment is needed for shaping into desirable shape; therefore, it is not amenable for easy fabrication [3].

2.3.3.2 LWCT Phantoms

The first phantom to simulate fat and bone has been introduced in the early 70s by Guy [39]; it consisted of laminac polyester resin, catalyst, acetylene black, and aluminum powder. By changing Acetylene black ratio it is possible to control the conductivity, while

varying the aluminum powder ratio is used to control the dielectric constant. The results show close resemblance of the human LCWT in literature [39]. However, this phantom did not achieve the wide application range the super stuff muscle phantom achieved, due some difficulties in the making and modeling [4].

Lagendijk and Nilsson [4] have made attempts to convert Guy's muscle phantom to simulate a fat phantom by adding more polythene powder (since it lowers the permittivity). Unfortunately, these attempts were unsuccessful. Another attempt was more successful to simulate LWCT. It was done by making a "dough", containing a weight ratio of 500:225:50, flour-oil-saline (0.9% NaCl per 1 Liter) respectively. The use of normal flour is to make the phantom manageable, since simulating low water tissue needs a low water ratio, and this might make the phantom too dry to handle. By changing the water content, the dielectric constant ε' can be controlled, but over 8%, the oil content must be lowered to keep the phantom manageable. The complex permittivity of this mixture was measured using a cylindrical TM010 at frequency 451.3MHz. The results proved successful simulating fat and bone tissues [4], ($\varepsilon^* = 7.3 - j1.5$) at 451 MHz.

Bini et al. [32] suggested new materials to simulate LWCT. The phantom was obtained by substituting the water content with non-polar or low permittivity liquid in the phantom formula. Several liquids have been tried, and successful results have been obtained with pyridine, dioxane and ethanediol (ethylene glycol). By using dioxane, the obtained phantom has very good mechanical properties and with high dioxane percentage, very low permittivity values can be obtained. However, the phantom found to be a white opaque was the one with a high percentage of dioxane. Care must be taken when using dioxine, since it is toxic by inhalation and moderately toxic by skin absorption. With reasonable care, it can

be handled easily and safely. The best results may be obtained with ethnediol and it simulates the fatty tissues well at frequencies between (0.75 - 5.5) GHz [45]. The phantom is found to be transparent, so it might be very useful in such applications where transparency is essential.

Another type of lower permittivity materials which has been reported to simulate fat is called EGP [33]. This phantom consists of ethanediol 55%, gelatin 5%, and polythene powder 40%. Since the polythene is stirred in a drop of detergent is added to help in wetting it. The measurement system consists of an open-ended coaxial cable sensor in conjunction with an automatic network analyzer, and a numerical analysis program has been used to determine the complex permittivity value. The results have been reported in a 3 frequencies :500, 1000, 2450 MHz. At 1000 MHz the value of the complex permittivity is ($\varepsilon^* = 8.2\text{-}3.6j$) which is slightly higher than fat tissues. The researcher suggested to substitute ethanediol with propanediol, since it is not possible to lower the permittivity by increasing the polythene powder content (as this weakness the material too much) [33]. The obtained phantom is rigidly formed in shape and soft to be cut by a knife.

Nikawa et.al. [2] have developed a "Dry phantoms" for simulating LWCT. It contains a raw silicon rubber, a curing agent and carbon fibers with two different grain sizes. Reflection method was used to measure the complex permittivity; the samples were shaped into toroidal shape and inserted into an open end coaxial cable. The reflection coefficient of the samples was measured by a network analyzer HP8752A, and then rechecked using a HP85070A dielectric probe for conformation, and the result was found to be almost similar. Reported results show that carbon fiber increases the relative permittivity and the loss factor, therefore, by choosing proper weight ratios of carbon fibers it is possible to simulate

LWCT. This phantom is easy to model and it is superior in preservation. However, this phantom is difficult to fabricate [3].

2.3.3.3 Materials Used for Simulating HWCT & LWCT:

There are phantoms that can be used to simulate both the tissues types, by using the same ingredients. Nikawa et al. [2] have proposed a dry phantom that is able to simulate HWCT and LWCT by varying two of the carbon type ratios [2].

More recently, another phantom, which is suitable to simulate both HWCL and LWCT has been introduced by Mariya Lazebnik et al. [49]. This phantom was based on oil-in-gelatin dispersions, and by changing the oil ratio, a wide band of the permittivity values can be obtained. To confirm the long time stability for this phantom, the measurements were repeated after two months on the same sample and the results shows a good shelf life for 6 weeks.

The main advantage of this phantom is the ability to manufacture heterogeneous construction with direct contact without change in the dielectric properties with time, because of solute or solvent diffusion [5]. Another advantage of this phantom is that it can be used for wide band frequency range of 0.5 GHz to 20 GHz, which makes it suitable for ultra wideband imaging application in breast cancer detection.

From all the above reviewed studies, it is easy to conclude that all the reviewed phantoms suffer at least one of these problems: stability over time, hard shaping, complex procedure of making, or no equation for the phantom to adjust the dielectric properties to match several published data on tissues.

2.4 Permittivity Mixing Equations of Heterogeneous Systems

2.4.1 Introduction

A heterogeneous system is a system composed of multi-constituent materials, typically a two phase composite dielectric constituted by, a host (matrix) material and inclusion (filler) of another material. The host-inclusion may be formed by dielectric-dielectric, semiconductor-dielectric or dielectric-conductor. The dielectric properties of these types of mixture may be predicted by using suitable mixing equations. A general overview on these mixing equations is presented in the following sections.

2.4.2 Permittivity of Heterogeneous Mixtures

The electromagnetic dielectric responses of dielectric mixtures have been studied in the literature [52-61]. However, irrespective of the size, shape, volume fraction, or orientation of the phases, the effective (complex) permittivity (ε_{eff}), should always lie within the 2 values of $\theta\varepsilon_1+(1-\theta)\ \varepsilon_2$ and $1/[\theta/\varepsilon_1+(1-\theta)/\varepsilon_2]$, those two limits referred to Wiener bounds [6]. Where ε_1 is the complex permittivity of the inclusion, ε_2 is the complex permittivity for the host medium and θ is the volume fraction of the inclusion.

The first dielectric model of two phase system was due to Clausius and Mossottoi [6, 62], as shown below:

$$(\varepsilon_{eff}/\ \varepsilon_2) = (1+3\theta X_d) \tag{3}$$

Where $X_d = \theta\ (\ \varepsilon_1 - \varepsilon_2)\ /\ (\ \varepsilon_1 + 2\varepsilon_2)$.

However, in many cases the heterogeneous system has more heterogeneous characteristics that could not be described by the above equation, and such equations are developed empirically or semi-empirically.

Following the equation of Clausius-Mossottoi, Rayeigh obtained the following equation [52], given by:

$$(\varepsilon_{eff} - \varepsilon_2) / (\varepsilon_{eff} + 2\varepsilon_{eff}) = \theta(\varepsilon_1 - \varepsilon_2) / (\varepsilon_1 + 2\varepsilon_2) \quad (4)$$

Under the condition of $\theta << 1$ (small volume fraction)

Burggeman et al. [53] applied the Rayleigh equation to find a symmetrical equation that applicable to conductivity as well as complex permittivity. The equation is:

$$\theta (\varepsilon_{eff} - \varepsilon_1)/(2\varepsilon_{eff} - \varepsilon_1) = (1 - \theta) (\varepsilon_{eff} - \varepsilon_2)/ (2\varepsilon_{eff} - \varepsilon_2) \quad (5)$$

When the concentration of the inclusion is high, each particle will be surrounded by a mixture rather than by the component. Bottcher [55] applied the Onsgar model in the case of spherical particles to obtain the following formula:

$$(\varepsilon_{eff} - \varepsilon_2) / 3\varepsilon_{eff} = \theta (\varepsilon_1 - \varepsilon_2) / (\varepsilon_1 - 2\varepsilon_2) \quad (6)$$

From the general principles of statistics, an expression based on mathematical hypothesis was proposed by Lichtenecker and Rother [56]. This expression simulates the dielectric constant of a mixture containing filler with a very high dielectric constant value without any loss; the expression has the following form:

$$(\varepsilon_{eff})^k = \theta (\varepsilon_1)^k + (1 - \theta)(\varepsilon_2)^k \quad (7)$$

Where k is an exponent constant determined by the wave propagation mechanism through the inclusions in insulating medium. For K values covering the Wiener limits, it is known that k=1 when the filler distribution is perpendicular to the direction of the wave propagation, whereas k= -1, when the filler distribution is parallel to the direction of the waves [57]. For k=1/3 the Looyenga's equation is found [58], that is when the inclusions are randomly dispersed at low concentration.

By numerical simulation, Stölzle et al. [59] have deduced an expression strongly related to Equation 6, to account for the effect of particle interaction with increasing volume concentration by introducing the exponent k as a function of θ, where:

$$k(\theta) = (1.65 \pm 0.05)\,\theta + (0.265 \pm 0.005) \tag{8}$$

Van Beek et al. [60] reviewed approximate equations derived from the formula for composite permittivities to predict the dielectric constant of a conductor-insulator system. These formulas were derived when ε of the conducting phase tends to infinity [54]. With this assumption, the well known equation could be applied as Bruggeman's formula et al. [53], Corkum's equation et al. [63] and Shin's et al. [64].

2.4.3 Epoxy - Carbon Black Mixtures Predictions at Microwave Frequencies of 1 GHz to 10 GHz

Different researchers investigated dielectric properties of heterogeneous systems nearly a hundred years ago, and many theories and empirical formulas were proposed to predict permittivity of heterogeneous systems [52-61]. In this section, a review on attempts to predict Epoxy- CB systems by using different developed equations is presented.

Achour et al. [54] reported the dielectric behavior of epoxy- CB at microwave frequency. The samples of their study were composed of two nearly spherical 2 types of CB, namely, Monarch 700 and Sterling, which are produced by Cabbot.Co. The CB was randomly dispersed in insulating Epoxy (diglycidyl ether of bisphenol A) produced by DEGBA, Ciba Geigy. Co. The complex permittivity of the manufactured samples was measured by the reflection coefficients technique at microwave frequency. In their study the experimental values of the complex permitivities were compared with those obtained by using different mixture laws (Maxwell-Garnett, Bruggeman, Bottcher, Lichtenecker, Lichtenecker and Rother, Looyenga, Stolezle and Shin equation). A comparison between the observed and predicted data concluded that the results of all the used mixture laws did not agree with the experimental data and it failed to interpret the dielectric behavior of the mixture. However, the best fit results could be obtained separately by using the Looyenga equation ($(\varepsilon^*)^k = \Phi(\varepsilon_c^*)^k + (1 - \Phi)(\varepsilon_m^*)^k$, where ε^*_c permittivity of conductor and ε_m^* for matrix) for the real part and Lichtenecker equation ($\ln(\varepsilon^*) = \Phi \ln(\varepsilon_c^*) + (1 - \Phi)\ln(\varepsilon_m^*)$)for the imaginary part of the permittivity.

Another attempt to predict the complex permittivity ($\varepsilon^* = \varepsilon' - j\varepsilon''$, where $\varepsilon'' = \sigma / \varepsilon_0\omega$) by using mixing equation had been done by Kim et al. [57]. The composite materials were manufactured using compounds composed of 4 wt % of CB (XE2 grade) produced by DEGUSSA and 96 wt % of Epoxy resin YD115 from KUKDO, which were mixed by a three-roll mill. In this study, six composites with different weights of CB were then manufactured by diluting the compounds with the YD115 and the hardener KBH 1089 from KUKDO. The mixing ratio (weight) between resins to hardener was 10:9 respectively. The concentration of the CB was calculated using the densities of resin (1.2 g/cm^3), CB (1.87 g/cm^3) and the weight content of the CB within the composites. The dielectric

measurement was done using Agilent N5230 A (PNA-L Vector Network Analyzer) on frequency range (0.5 - 18) GHz. In the complex permittivity prediction, a formula was used after implementing a correction factor z to the Lichtenecker-Rother equation. The new modified formula could be found in the following form:

$$(\varepsilon^*)^k = z\,p\,(\varepsilon^*_1)^k + (1 - z\,p)\,(\varepsilon^*_2)^k \quad (9)$$

Where ε^*, ε^*_1 and ε^*_2 are the complex of a composite, filler, and the matrix material, respectively. K is expressed as $k = Ap + B$, where A, B, and z are functions of frequency that were obtained numerically from the experimental results and calculated by the following equations:

$$A = 11\,f^{0.0208} - 14.748 \quad (10)$$

$$B = -0.22\,f^{0.0537} + 1.0582 \quad (11)$$

$$Z = 3.23\,f^{0.0416} - 6.481 \quad (12)$$

The conductivity of the CB used in this study found to be 4100 S/m, and the dielectric constant is 2.75, which is the static value for most common kinds of carbon black.

The results of the prediction equation then were compared with the experimental values. The Comparison showed good agreement between both the experimental and the prediction results. Figure 2.5 and Figure 2.6 Demonstrate that [57].

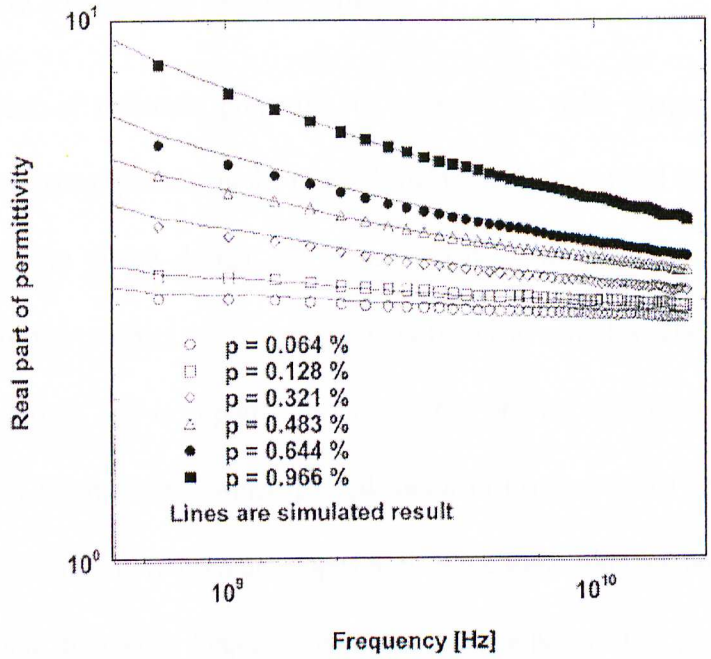

Figure 2.5 The comparison of the frequency spectrums of the dielectric constants of carbon black/epoxy composites from experimental values and simulated results of eq. (9).

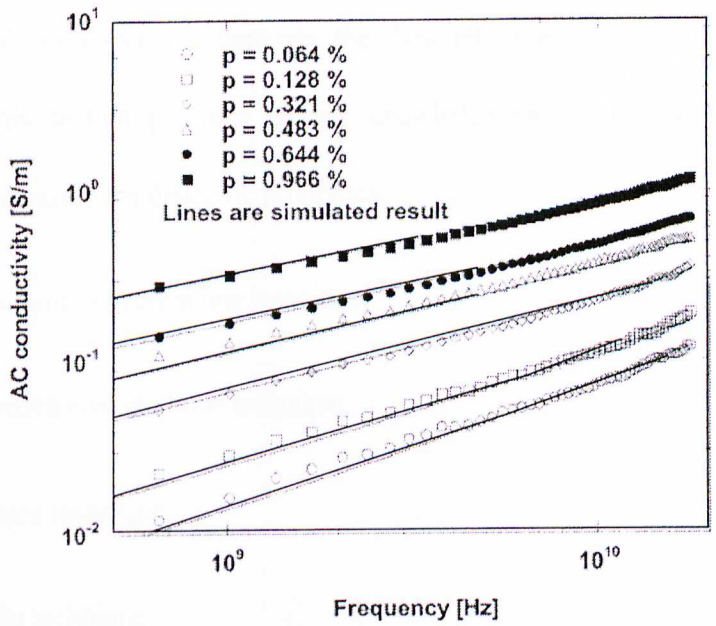

Figure 2.6 The comparison of the carbon black concentration dependency of the electrical conductivities of carbon black/epoxy composites from experimental values and simulated results of eq. (9).

2.5 Dielectric Properties Measurements

The measurement of dielectric properties of materials at radio frequency has gained increasing importance especially in the research fields, such as material science, biological research, microwave circuit design, etc. Measurement of dielectric properties involves measurements of the complex relative permittivity (ε^*_r) and complex relative permeability (μ^*_r) of the materials, and is important because it can provide the electrical or magnetic characteristics of the materials, which proved useful in many research and development fields. Many techniques have been developed to measure these complex properties such as techniques in time domain or frequency domain with one port or two ports, etc [65-67]. Every technique is limited to specific frequencies, materials and applications by its own constraint. With the advance of new technologies, the techniques can be employed with a software program that measures the complex reflection and transmission coefficients with a Network Analyzer (NA) and converts the data into the complex dielectric property parameter. This section provides general knowledge on the following four common techniques to measure the dielectric properties:

- transmission/reflection line technique,
- open ended coaxial probe technique,
- free space technique
- resonant technique

Table 2.1 describes some examples of materials, s-parameters and dielectric properties measured using various measurement techniques.

Table 2.1 Comparison between the measurement techniques [65]

Measurement techniques	Materials	S-parameters	Dielectric properties
Transmission/Reflection Line	Coaxial line, waveguides	S11, S21	ε_r, μ_r
Open-ended coaxial probe	Liquids, biological specimen, semi-solids	S11	ε_r Where $\mu_r=1$
Free space	High temperature material, large flat solid, gas, hot liquids	S11,S21	ε_r, μ_r
Resonant Technique (Cavity)	Rod shaped solid materials, waveguides, liquids	Frequencies, Q-factors	ε_r, μ_r

2.5.1 Transmission/Reflection Line Technique

A measurement using the Transmission/Reflection line technique involves placing a sample in a section of waveguide or coaxial line and measuring the two ports complex scattering parameters with the NA. Calibration must be carried out before making the measurement. The technique involves measurement of the reflected (S11) and transmitted signal (S21). The relevant scattering parameters are related closely to the complex permittivity and permeability of the material. The conversion of s-parameters to complex dielectric parameters is computed by using a program [65]. In many cases, the technique requires

sample preparation such as machining so that the sample fits tightly into the waveguide or coaxial line in order to reduce measurements uncertainties caused by air gabs. Figure 2.7 shows the Transmission/Reflection Line technique using NA.

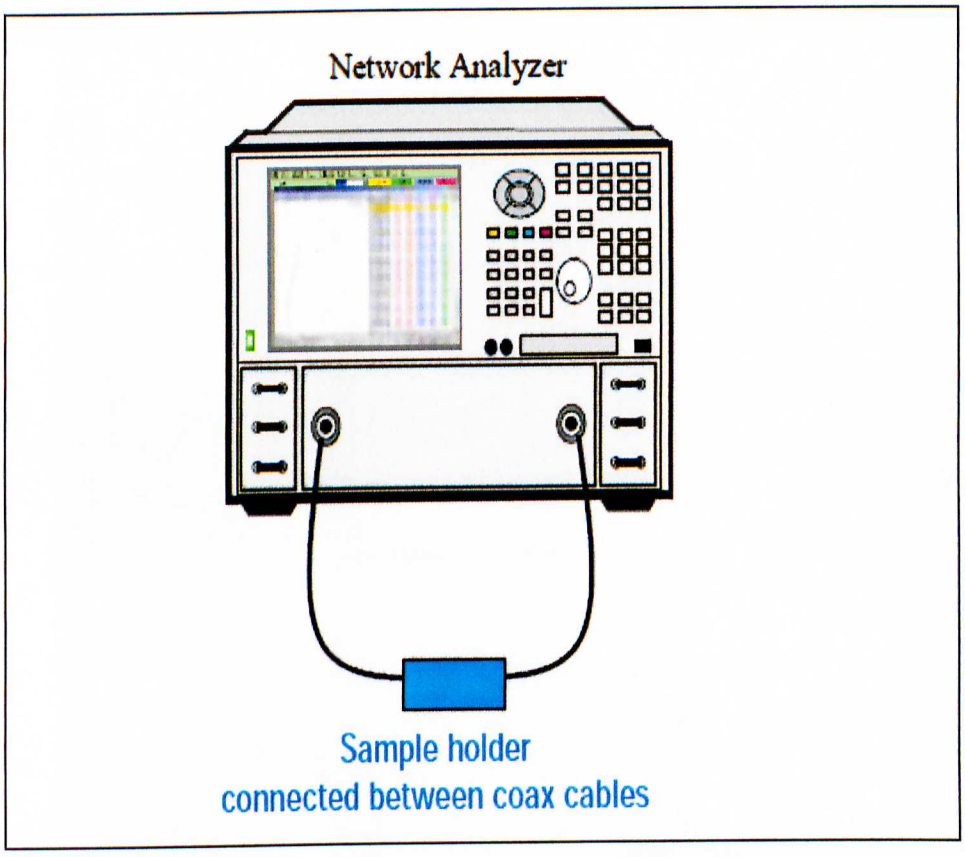

Figure 2.7 Dielectric properties measurements using transmission/reflection line technique [72]

2.5.2 Open Ended Coaxial Probe Technique

Open ended coaxial probe technique has been used for years as a non-destructive testing method [33, 65, 67]. In this technique, the probe is pressed against a specimen or immersed into the liquids, and the reflection coefficient is measured and used to determine the permittivity. Furthermore, for some measurements, it may not be possible to cut out the sample of a material for measurement. This is especially important in the case of biological specimens to perform in-vivo measurements because the material characteristics may

change. Therefore, with this technique the sample can be placed in close contact with the probe without causing any changes in the material characteristics [65]. The reflection coefficient is measured using NA. The NA with a probe system is first calibrated so that the reflection coefficient measurements are referenced to the probe aperture plane. Figure 2.8 demonstrates the dielectric properties measurements using open-ended coaxial probe technique.

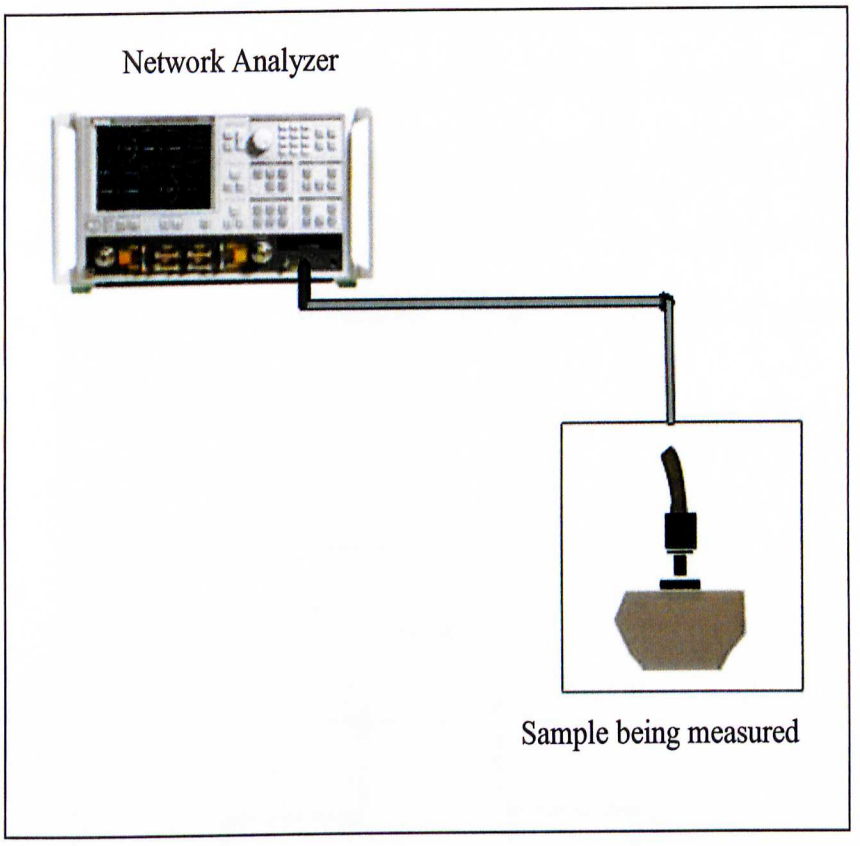

Figure 2.8 Dielectric properties measurements using open-ended coaxial probe technique [72]

2.5.3 Free Space Technique

Free space measurement allows measurements on the Material Under Test (MUT) under high temperatures or hostile environments and generally operates in wide band frequencies.

The measurement requires the MUT to be large and flat. It usually utilizes two antennas placed facing each other and the antennas are connected to a network analyzer. Once calibrated, the s-parameters of an empty sample holder are measured by placing the sample holder midway between the two antennas. The MUT is then placed on the sample holder between the antennas and the s-parameter measurement is performed again as shown in Figure 2.9. Using the de-embedding function of the VNA, the influence of the sample holder can be cancelled out and only the s-parameter of the MUT can be determined.

The s-parameter for both the reflection and transmission coefficients can be determined. Time domain gating should also be applied to ensure there are no multiple reflections in the sample itself, though appropriate thickness should enable to avoid this. It also eliminates the diffraction of energy from the edge of the antennas. The dielectric properties can be determined by post processing the measured reflection and transmission coefficient using a program [65].

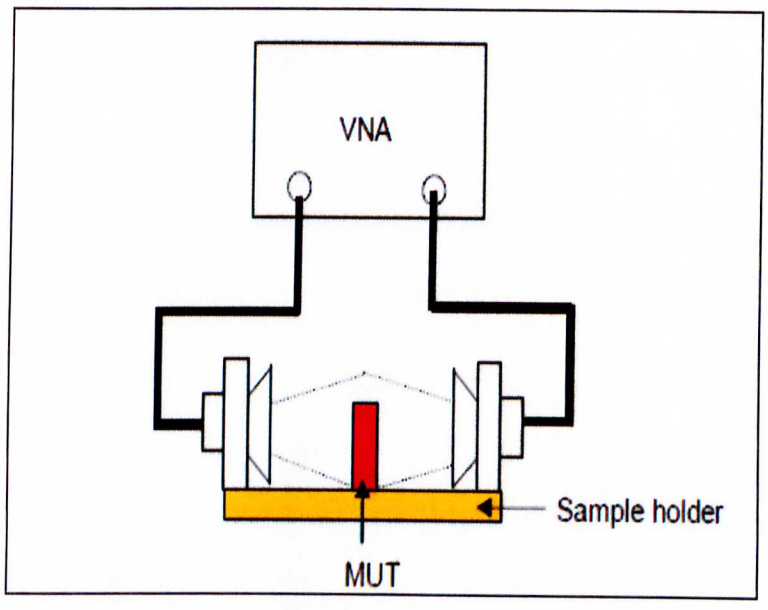

Figure 2.9 Dielectric properties measurements using free space technique [65]

2.5.4 Resonant Technique

Resonant measurements are the most accurate methods of obtaining permittivity and permeability especially for low loss materials [66]. However, there are limitations on the frequencies and loss characteristics of the materials that can be measured with the technique. There are many types of resonant techniques available such as reentrant cavities, split cylinder resonators, cavity resonators, fabry-perot resonators etc. There are two types of resonant measurements commonly used. Perturbation methods are suitable for all permittivity measurements, magnetic materials and medium to high loss material measurements. Low loss measurement method is a measurement on low loss materials using larger samples. However, the perturbation method is more popular with resonance characteristics depending on the MUT in a cavity; its quality factor and resonance frequency can be monitored to determine the dielectric parameters. The dielectric properties can be determined by first measuring the resonant frequency and quality factor of an empty cavity.

The second step is to repeat the measurement after filling the cavity with the MUT. The permittivity or permeability of the material can then be computed. There is no need to calibrate the network analyzer for this type of measurement [65]. Figure 2.10 illustrates the measurements by using resonant cavity technique.

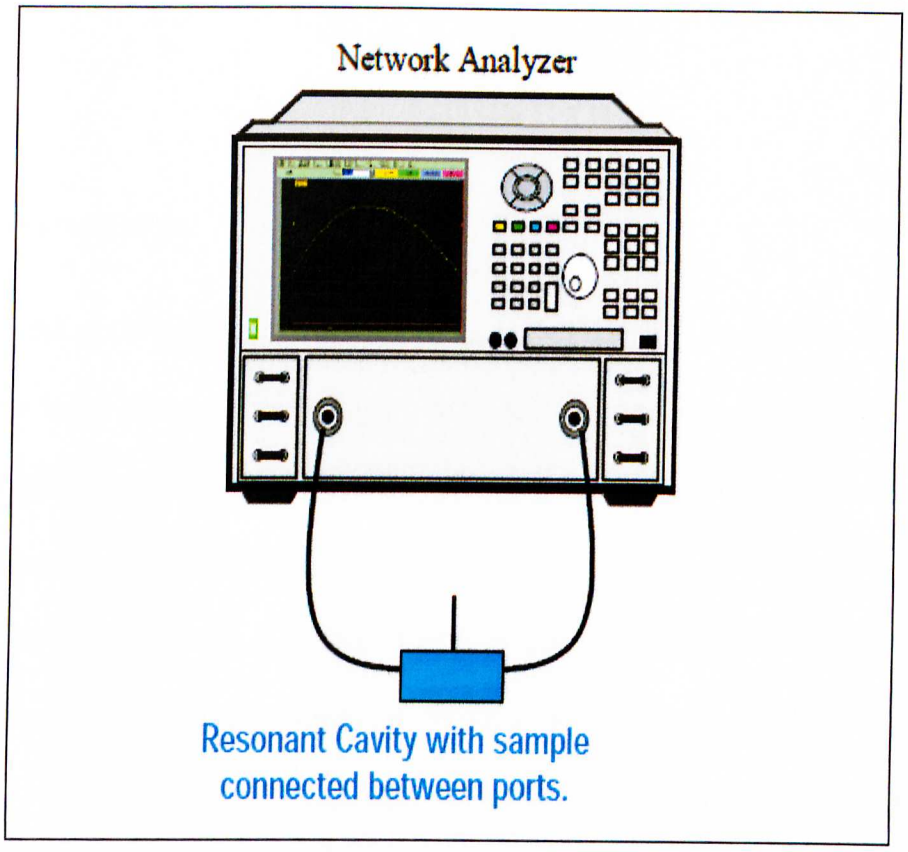

Figure 2.10 Dielectric properties measurements by using resonant cavity technique [66]

CHAPTER 3

METHODOLOGY

3.1 Introduction

Briefly, the methodology of this research is shown in Figure 3.1. It starts with applying the equation in the Microsoft Excel Program to calculate the complex permittivity. Next step was to adjust the ratio of the Carbon Black (CB) to obtain the optimum ratios that approach the dielectric properties of human tissues. Several experiments were conducted in order to manufacture samples with the obtained ratio from the equations. This was followed by measuring the complex permittivity of the samples by using Network Analyzer (NA) measurements. These values were compared with the theoretical values obtained from the equation.

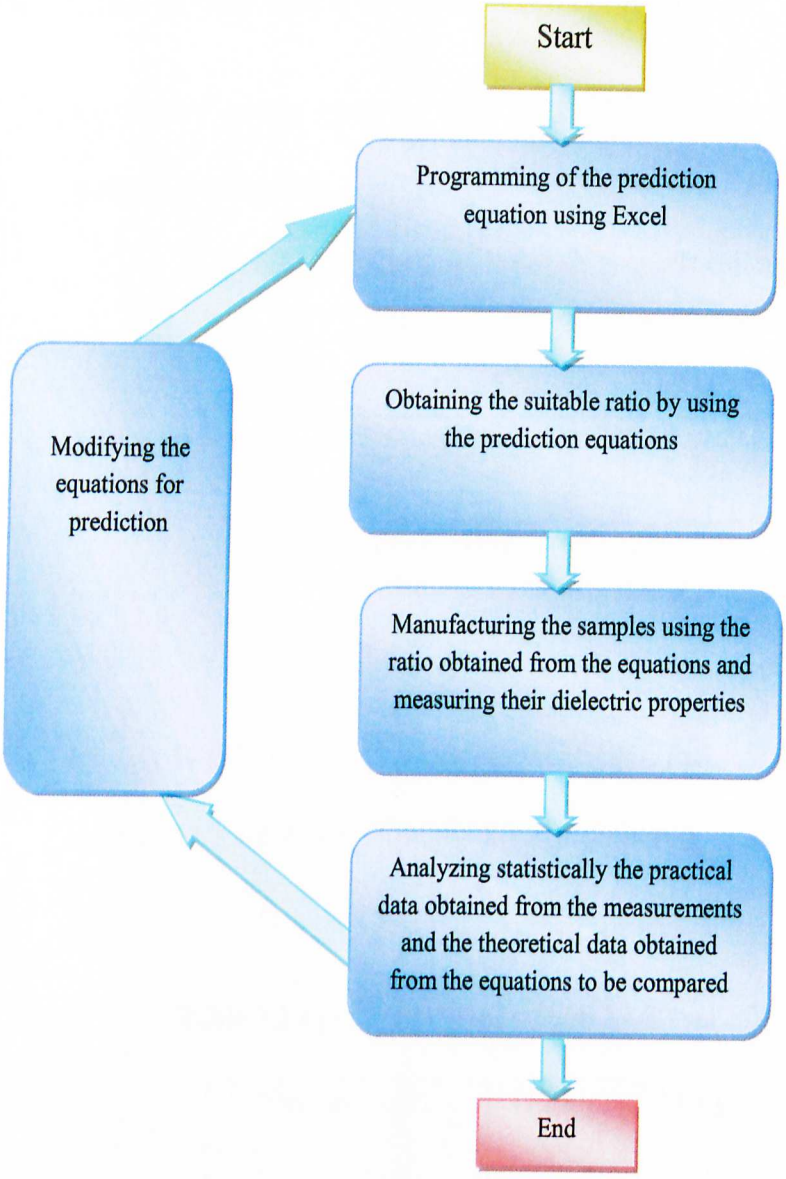

Figure 3.1. Flow chart for project methodology

3.2 Materials and Equipments

The materials that were used in the current study consisted of:

- Conductive carbon black of XE2 grade (DEGUSSA). Table 3.1 presents the material specifications.

Table 3.1 Carbon black (XE2) specifications

Density	1.87 g/cm^3
DBP absorption	380 ml / 100 g
Dielectric constant	2.5 – 3.0

- Epoxy BONDITE 8950-1A/B (MIRACON (M) SDN BHD) Material's specifications are shown in Table 3.2.

Table 3.2 Epoxy (BONDITE 8950-1A/B) specifications

Density (A/B)	(1.25 g/cm^3 / 1.1 g/cm^3)
Mix viscosity	850 CPS
Mixing ratio (A/B)	100:50

The equipments used in this study consisted of:

- Computer software Microsoft Office EXCEL 2007
- Electronic balance ST-2004

- E8363 Agilent PNA Network Analyzer
- 85070E Agilent Dielectric Probe Kit With High Temperature Probe, Probe Stand
- Mounting Bracket, Ecal Holder and Adapter
- N4693A Agilent Ecal Module
- 34970A Data Acquisition Unit with 34901A 20-Channel Multiplexer
- RF cable
- Bottled water
- Dry towel paper

3.3 Sample Preparation

This starts with applying the prediction equation in Excel to calculate the concentration of the CB that mixed with the Epoxy to obtain the dielectric properties that are similar to fat tissues. The equation used is as follows:

$$(\varepsilon^*)^k = z\,p\,(\varepsilon^*_1)^k + (1 - z\,p)\,(\varepsilon^*_2)^k \tag{9}$$

Where ε^*, ε^*_1 and ε^*_2 are the complexes of the composite, filler, and the matrix material, respectively. K is expressed as $k = Ap + B$, where A, B, and z are given by:

$$A = 11\,f^{0.0208} - 14.748 \tag{10}$$

$$B = -0.22\,f^{0.0537} + 1.0582 \tag{11}$$

$$Z = 3.23\,f^{0.0416} - 6.481 \tag{12}$$

Composite samples used in this study were manufactured using paste that is composed of 5 wt % of CB and 95% Epoxy resin. The paste was prepared as follow:

First, epoxy resin and conductive powder were mixed thoroughly using high speed mixer at 500 rpm. Once the mixture has been thoroughly dispersed, the mixture of epoxy resin with conductive powder was poured into a grinding machine. As the grinding process continues, the grinding machine ground the mixture of epoxy resin with conductive powder into a fine mixture in paste form. A spatula was used to scrape down the mixture from the blade and collect the conductive paste in a container.

Samples with a variety of CB weight contents were manufactured by diluting the paste with the resin. The total resin in the composite was 100 g. Table 3.3 presents CB concentration (P), of the fabricated samples, where the concentration was calculated using densities of epoxy (1.25 g/cm^3), CB (1.87 g/cm^3) and the weight content of CB within the composite sample.

The P values in Table 3.3 were found using the volume concentration equation as follows:

$$P\ \% = 100 * V_{CB} / (V_{CB} + V_{Resin}) \quad (13)$$

Where V is Voume (Voume= Weight/Density). Below are examples of P calculations for S1 and S2.

P (S1) % = 100 * 0 g % / [0 g % / 1.87 g/cm^3 + 100 % / 1.25 g/cm^3] = 0 %

P (S2) % = 100 * 0.54803008 g % / [0.54803008 g % / 1.87 g/cm^3 + 99.452 % / 1.25 g/cm^3] = 0.3669 %

Table 3.3 Volume fraction of components in samples

Sample Name	Weight fraction of CB (wt %)	Concentration of CB (P %)	Concentration of Epoxy Resin (%)
S1	0	0	100
S2	0.54803008	0.3669	99.452
S3	0.776178345	0.5201	99.224
S4	0.949007559	0.6363	99.051
S5	1.25621839	0.8432	98.744
S6	1.563181598	1.0503	98.437
S7	1.79679941	1.2082	98.204

Then an amount of 26.666 g of resin and 63.333 g of hardener were added to the sample. The overall mixing ratio (weight) of the resin and the hardener was 10:5 in each sample. The mixture was mixed by stirring at 50 rpm for 15 min as illustrated in Figure 3.2.

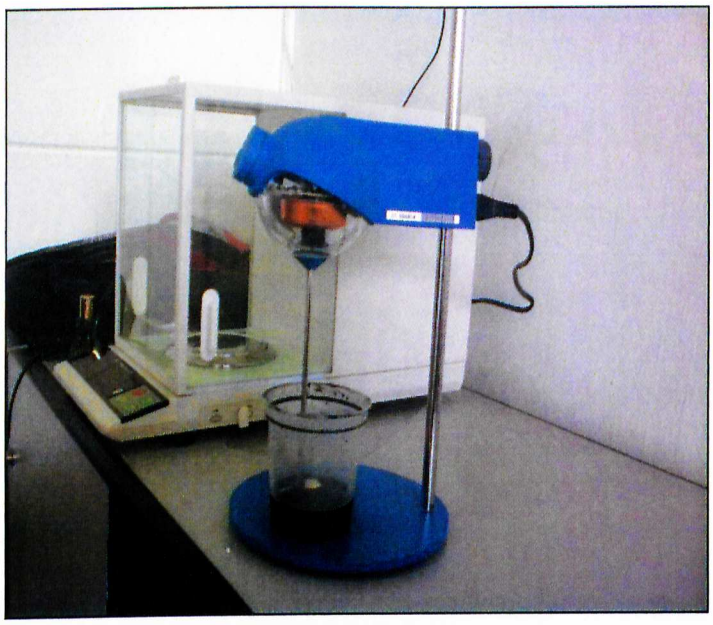

Figure 3.2 The mixing of the epoxy and CB

After extracting the vapors from the material by using a vacuum machine, the diluted mixtures were poured into the molds at atmospheric pressure and left for 24 hours to cure. Finally, the samples were shaped and their surfaces were smoothed for the dielectric properties measurements as demonstrated in Figure 3.3.

Figure 3.3 Prepared samples after smoothing and shaping for the dielectric properties measurements

3.4 Data Collection

Relative dielectric constant $\acute{\varepsilon}_r$ and conductivity σ were measured using Network Analyzer (Agilent E8363) with Agilent Dielectric Probe Kit 85070E at frequency range 1 GHz to 10 GHz. The measurement procedure as follows:

1. All equipment was turned on and warmed-up for about 1 hour before use. Figure 3.4 shows the used equipments.

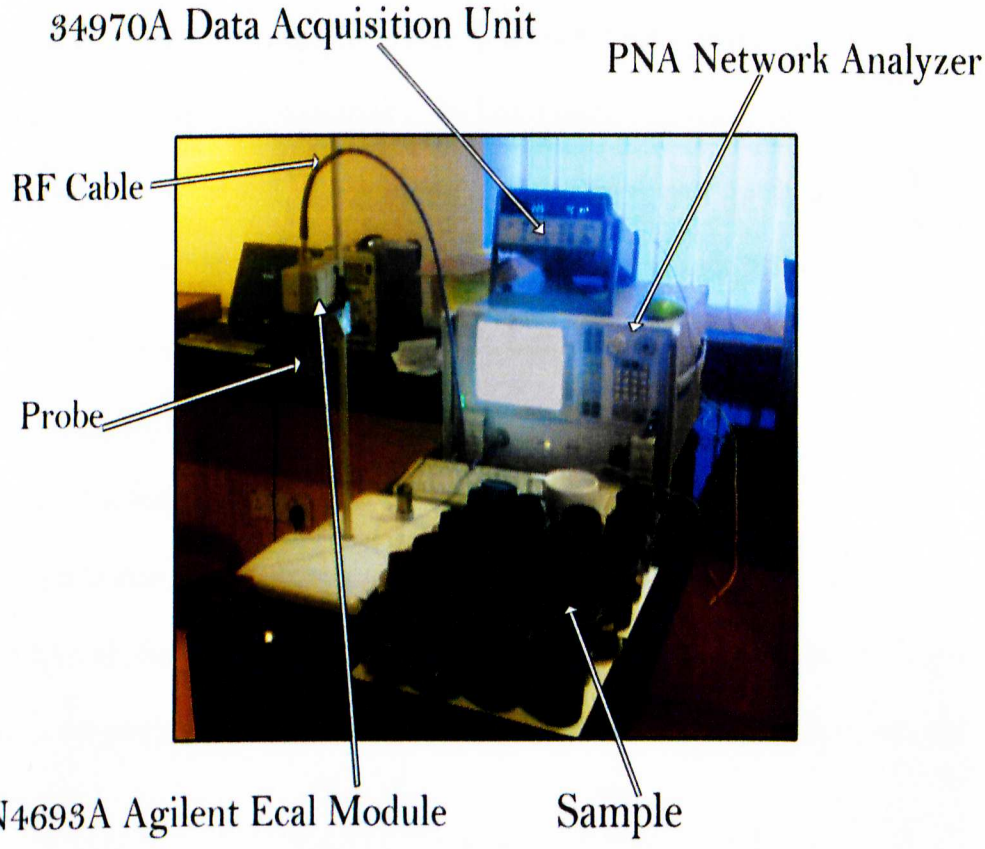

Figure 3.4 The used equipments for the dielectric properties measurements.

2. The mounting bracket was connected to the probe stand by slipping the opening over the Probe Stand rod, and tightening the two large thumb screws in the back.

3. The ECal Holder was connected to the mounting bracket using screws from the mounting bracket and tightening with a Hex Key.
4. The ECal module was fitted into The Ecal Holder (Note: the fit is tight to make sure Ecal is secure)
5. A Large knurled nut was removed from the connector end of the high temperature probe.
6. The connector end of the probe was guided up through a hole in the mounting bracket and was then connected to Ecal.
7. An RF cable was connected between the ECal module and network analyzer.
8. An ECal USB cable was connected to the USB port on the network analyzer.
9. All equipment, water and MUT were left to allow temperature to stabilize.
10. The stabilized temperature was measured and recorded using the 34970A.
11. The 85070E software was launched from the network analyzer.
12. The frequency range was set from 200 MHz to 10 GHz, linearly spread over 1001 points. [Calibration ▶ Set Frequency]
13. The calibration was configured to be Air/Short/Water (Calibration Type) (Figure 3.5), ECal Module (Refresh Standard Type), High Temperature (Probe Type) and water temperature recorded from step 10 was keyed in. [Calibration ▶ Configure Cal]

Figure 3.5 The NA calibration using distilled water at room temperature.

14. Calibration was performed according to the software prompt using air, high temperature probe short and water. [Calibration ▶ Perform Cal] (Note: always ensured probe was dried after doing water calibrations or measurements)
15. Permittivity measurements were done for water and air [Measure ▶ Trigger Measurement] and the respective data files were saved [File ▶ Include Sensitivity Data, Save Data File].
16. Permittivity of air was stored into Memory 1. [Display ▶ Data -> Memory ▶ Memory 1]
17. Normalization to permittivity of air was performed for MUT measurements to improve accuracy. [Display ▶ Trace Math ▶ /ref, Memory 1]
18. The probe face was pressed down as flat as possible on the surface of the MUT to ensure gap-free contact.

19. Permittivity measurement of the MUT was performed on three different locations on the surface of the MUT and each data file was saved.
20. Steps 18 to 19 were repeated until all MUTs were done.
21. All data was tabulated and plotted onto graphs.

Figure 3.6 and 3.7 show how the measurement of the dielectric properties was carried out.

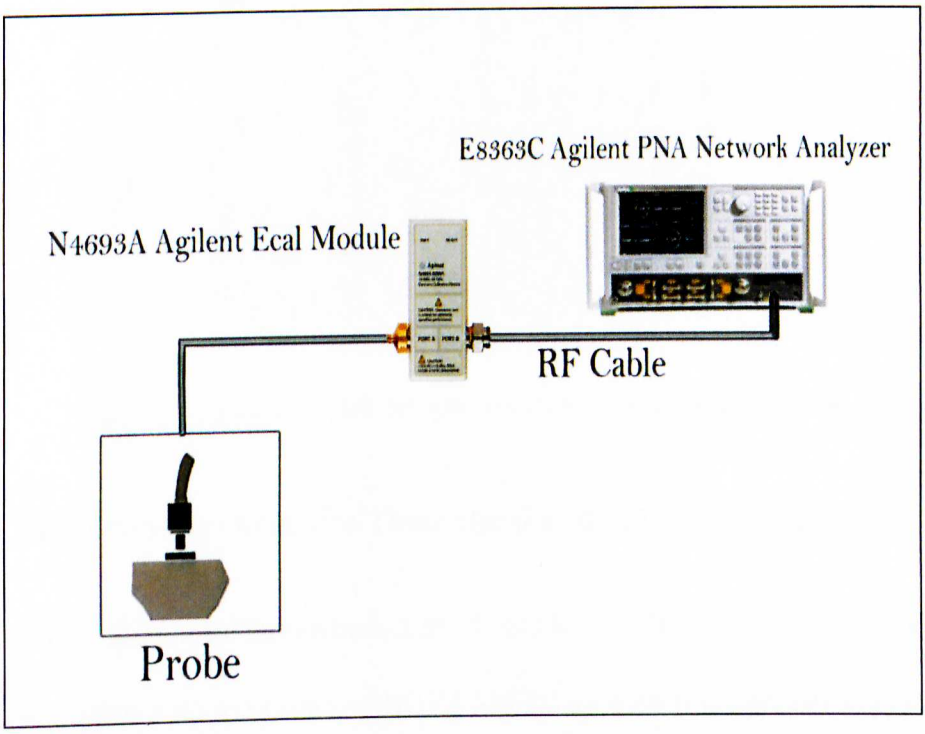

Figure 3.6 Block diagram in general of the dielectric properties measurements

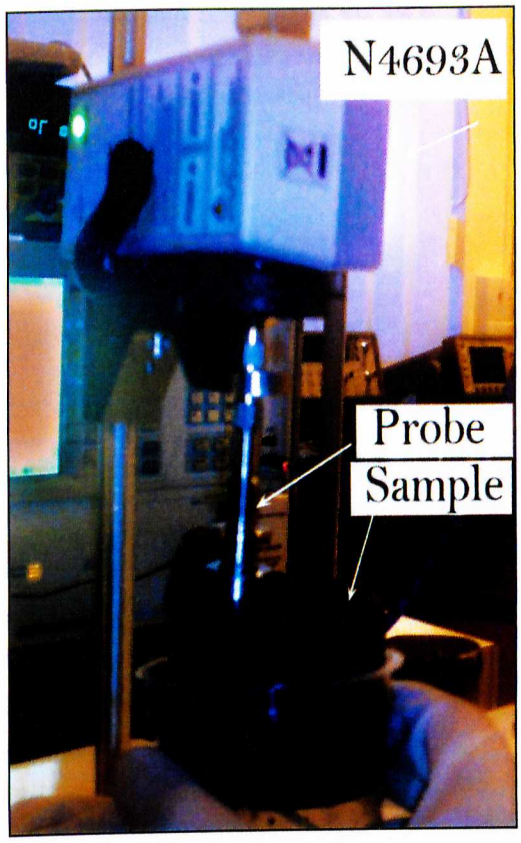

Figure 3.7 The dielectric properties measurements in progress

3.5 Comparison between the Theoretical and the Practical Results

The data from the sample measurements and theoretical results were analyzed using SPSS statistical program such as One-way ANOVA and Paired t-test (Independent Sample t-test) to evaluate the diverging between them. To carry out the right and acceptable statistical test, we have to consider:

1. Type of data (Interval, ratio o f nominal)
2. Research questions
3. Assumption of the statistical tests (Homogeneity of variance)

One-way ANOVA was used to evaluate the significant difference between samples at different bandwidth. One-way ANOVA is a robust technique for the violation of assumption of homogeneity of variance (If the data violate the assumption, multiple

comparison tests that do not assume equal variances are used such as Tamhane's T2, Dunnett's T3, Games-Howell, Tuky and Dunnett's C). To assess homogeneity of variance Levene test is used. The results of Levene test determines which type of Post-hoc technique are suitable. Tukey's post hoc test was used if there was an equality of variances. Dunnette's T3 post hoc was used if there was non-equality of variances observed, where Independent Sample t-test was used to differentiate between two groups of data.

The coefficient of variation (CV) of a single measurement is determined by the variability of the data and the experimental error. Continuous variables that have a coefficient of variation (CV = standard deviation / mean) less than 20% is always an indication of acceptable experimental errors.

Since wide diverges occur between the practical and theoretical data curves, which was confirmed by Independent Sample t-test. Therefore, a correction factor was applied to the equation to improve its prediction performance. Then the prediction performance was tested again using Independent Sample t-test.

CHAPTER 4

RESULTS & DISCUSSIONS

4.1 Introduction

The results of the permittivity and conductivity measurements for each of the samples are presented and discussed in precedent subtitles. Theoretical (calculated) and practical (measurement) results were compared; however, the values of the theoretical results were in disagreement with the practical. Therefore, the theoretical equation was then enhanced by a correction factor. A comparison between the modified and the practical results was again analyzed.

One-way ANOVA analysis was used to compare the results of the permittivity and the conductivity versus frequency and concentration. Prior to One-way ANOVA, an analysis of the Levene's Test of Equality of Error Variances was used to check the equalities of variance of the samples. If there was an equality of variances, Tukey's post hoc test was used, where the test gave a p-value of more than 0.05 (homogeneity acceptable). While, if there was non-equality of variances observed, Dunnette's T3 post hoc was used, where the test gave a p-value of less than 0.05 (homogeneity is not acceptable).A paired t-test was also used to compare between the theoretical values before the modification and practical results. After the equation modification, the paired t-test again was used to compare it with the practical results.

4.2 Sample Measurements Results of Permittivity and Conductivity

Results of the relative dielectric constant (permittivity) and the conductivity measurements made by Network Analyzer (Agilent-E8363) are presented below in Figure 4.1 and 4.3 respectively, while Figures 4.3 and 4.4 shows permittivity and conductivity with various concentrations at selected frequency.

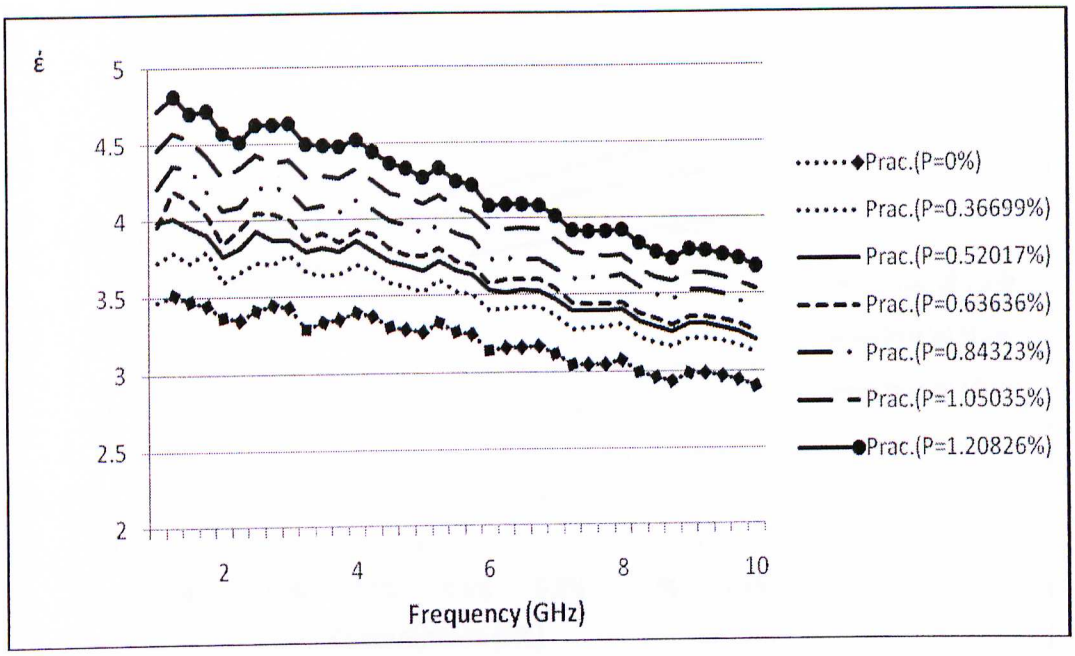

Figure 4.1 Permittivity measurements at frequency (1-10) GHz

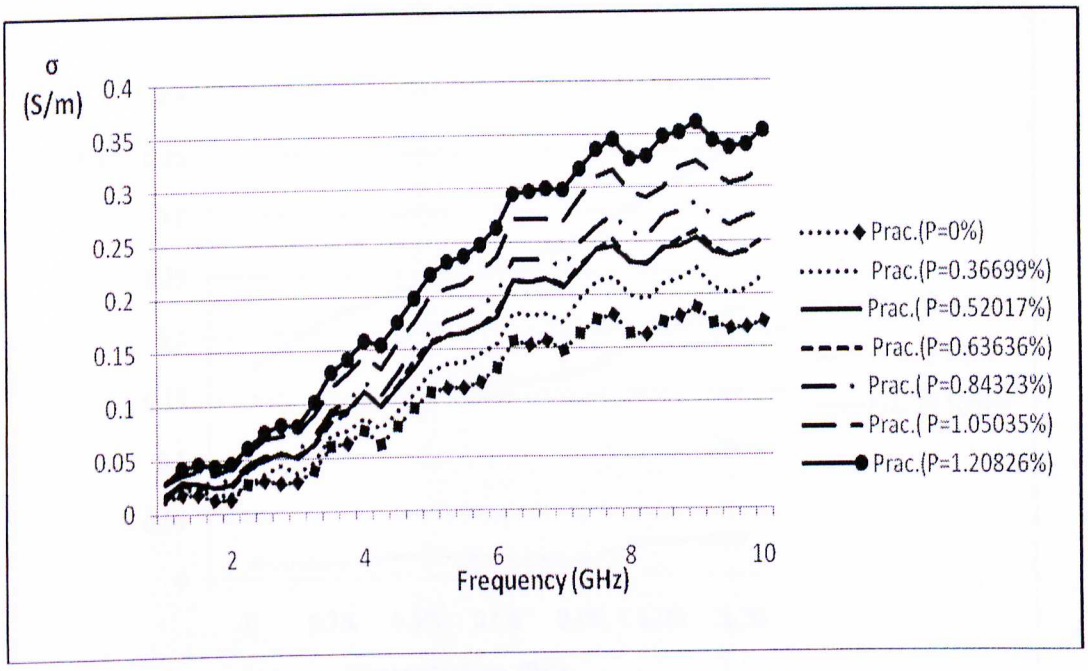

Figure 4.2 Conductivity measurements at frequency (1-10) GHz

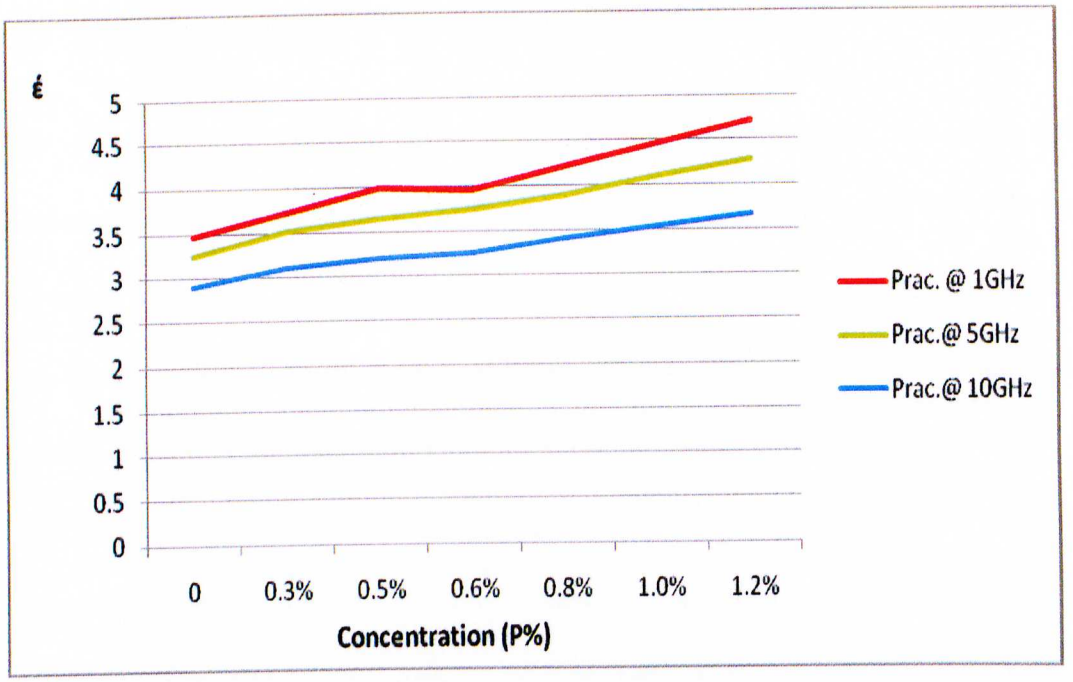

Figure 4.3 Permitivity with various concentrations at selected frequency

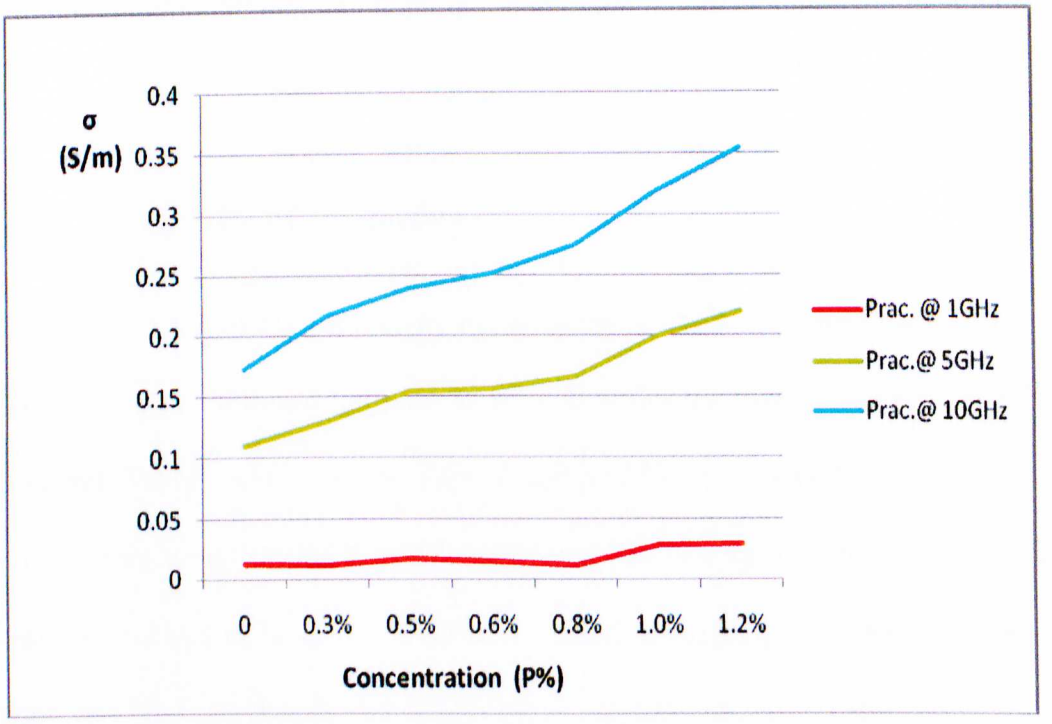

Figure 4.4 Conductivity with various concentrations at selected frequency

4.3 Statistical Analysis of the Practical Results

The practical results of the permittivity and conductivity of the frequency and concentrations analyzed statistically using One-way ANOVA. It was carried out by taking the mean value of the permittivity and conductivity curves then comparing between these two values. Levene's Test of Equality of Error Variances was carried out after taking the significant result of One-way ANOVA, and then it was used to check equality of variances. Tukey's post hoc test or Dunnette's T3 post hoc multiple comparisons are used to differentiate separately between the concentration levels and frequencies of the permittivity and conductivity. The Paired-Samples t-test procedure was carried out by comparing the means of two variables for a single group. Then the procedure computes the differences between values of the two variables for each case and tests whether the average differs from 0.

4.3.1 Permittivity by Frequency

The Levene's test of the permittivity by frequency in Table 4.1 shows that equality of variances can be assumed, (significant value is 0.739, i.e p-value greater than 0.05). Therefore, Tukey's post hoc test was used to compare the practical results of permittivity at various frequencies (Table 4.2), and then One-way ANOVA was used to show the overall result as presented in Table 4.3. Where Df1 and Df2 are degrees of freedom, F represents F-test, and Sig. is p-value.

Table 4.1 Levene's Test of Equality of Error Variances of the permittivity by frequency

F	Df1	Df2	Sig.
.547	5	36	.739

Table 4.2 Tukey's post hoc multiple comparisons show ε at different frequency. The values in the frequency range of 6 GHz to 10 GHz have no significant difference. Other ranges of frequency give non-significant difference, which are 2 GHz to 8 GHz and 1 GHz to 6 GHz. It is also noticed from the Table 4.2 that the permittivity values decreases as the frequency increases.

Table 4.2 Tukey's post hoc test of the permittivity by frequency

Frequency (GHz)	N	Subset for alpha = 0.05		
		1	2	3
10	7	3.297886		
8	7	3.502100	3.502100	
6	7	3.627143	3.627143	3.627143
2	7		3.926914	3.926914
4	7		3.978814	3.978814
1	7			4.077386
Sig.		.516	.146	.191

Table 4.3 shows the result of One-way ANOVA for the analysis of the permittivity by frequency. The p-value is less than 0.05. Hence, permittivity significantly differs in at least one pair of frequencies.

Table 4.3 One-way ANOVA analysis of permittivity by frequency

	Sum of Squares	Df	Mean Square	F	p-value
Between Groups	3.293	5	.659	5.249	.001
Within Groups	4.517	36	.125		
Total	7.811	41			

4.3.2 Conductivity by Frequency

The Levene's test of conductivity by frequency in Table 4.4 shows that equality of variances cannot be assumed since the p-value is less than 0.05. Thus, Dunnette's T3 post hoc multiple comparisons test was used to compare the curves of the conductivity practical results at various frequencies, and then One-way ANOVA was used to show the overall result.

Table 4.4 Levene's Test of Equality of Error Variances of the conductivity by frequency

F	Df1	Df2	Sig.
4.349	5	36	.003

As shown by Dunnette's T3 post hoc multiple comparisons, the conductivity for 4 GHz, 6 GHz, 8 GHz and 10 GHz are significantly different compared to 1 GHz and 2 GHz. The conductivity for 6 GHz, 8 GHz and 10 GHz are significantly different compared to 4 GHz. The conductivity for 10 GHz is significantly different compared to 6 GHz. A Sample of Dunnette's T3 post hoc multiple comparisons is shown in the Appendix Table. Table 4.5

words, there are four ranges of CB concentration (0 % to 0.63636 %), (0.36699 % to 0.84323 %), (0.52017 % to 1.05035 %) and (0.84323 % to 1.20826 %) and there are no significant differences. It is also noted from the table that the permittivity value increased as the percentage of carbon black is increased.

Table 4.7 Tukey's post hoc test of the permittivity by concentration

		Subset for alpha = 0.05			
Concentration	N	1	2	3	4
0%	6	3.222517			
0.36699%	6	3.474350	3.474350		
0.52017%	6	3.622500	3.622500	3.622500	
0.63636%	6	3.665900	3.665900	3.665900	
0.84323%	6		3.860700	3.860700	3.860700
1.05035%	6			4.051317	4.051317
1.20826%	6				4.248000
Sig.		.210	.357	.243	.354

One-way ANOVA results are shown in the Table 4.8 where the p-value is less than 0.05. Hence, the mean permittivity value is significantly different in at least one pair of concentrations.

Table 4.8 One-way ANOVA analysis of permittivity by concentration

	Sum of Squares	Df	Mean Square	F	p-value
Between Groups	4.362	6	.727	7.379	.000
Within Groups	3.448	35	.099		
Total	7.811	41			

4.3.4 Conductivity by Concentration

The One-way ANOVA test in Table 4.9 shows that the p-value is more than 0.05. Hence, there is no significant difference in conductivity at various levels of concentration, which means that the concentrations of CB have a minor effect on the conductivity. Therefore Levene's or Tukey's Test were not used.

Table 4.9 One-way ANOVA analysis of conductivity by concentration

	Sum of Squares	Df	Mean Square	F	p-value
Between Groups	.045	6	.007	.642	.696
Within Groups	.405	35	.012		
Total	.450	41			

4.4 Discussion of the Measurement Results of Permittivity and Conductivity

Both $\acute{\varepsilon}_r$ and σ show opposite behavior, i.e. $\acute{\varepsilon}$ slightly decreases with the frequency while the σ increases with the frequency, as shown in Figures 4.1 to 4.4. These differences show that $\acute{\varepsilon}_r$ and σ have frequency dependence. It has been also proven statistically by One-way ANOVA, as shown in Table 4.2 for $\acute{\varepsilon}$, and in Table Dunnett T3 Multiple Comparisons in the Appendix Table for σ. It can be noticed, in Figures 4.1 to 4.4, that the frequency dependence of $\acute{\varepsilon}$ and σ was increased by the addition of the CB. These results have the same opinion with Moon et al. [68], who had measured the dielectric properties of epoxy and CB composites in order to develop dry phantom materials that are able to simulate human tissues. As the frequency increased, the time required for the interfacial charges to be

polarized or for the dipoles to be arranged is delayed, and thus this frequency dependence of έ can be shown [68]. Dependence of σ upon frequency is related to ε" (where $\sigma = \varepsilon'' \varepsilon_0 \omega$ [S/m]). Frequency dependence of ε" is usually described by the sum of two terms which are $\sigma_0 / \pi 2f$, accounting for conductive effects, and ε''_R , accounting for relaxation effects [54,69]:

$$\varepsilon'' (f) = \sigma_0 / \pi 2f + \varepsilon''_R \qquad (14)$$

When the material is subjected to an electric field, dipoles are induced at the interface and the loss factor frequency dependence can be explained by the relaxation of those dipoles [69].

It is generally known that the dielectric properties of fat tissues are low when compared to other types of tissues in the human body [5, 34, 37-38]. This low dielectric property of fat tissues is due to the littleness of water content in fat tissues. Figures 4.1 and 4.2 show that the dielectric properties of pure epoxy (P=0%) is quite near comparing to the published data of pure epoxy [57]. These values are even lower than the reported studies of fat tissues [35-38]. However, the curves of έ and σ rise with the increase of CB concentration at the same frequency in the experimental results. One-way ANOVA analyses in Tables 4.8 and 4.9 show that the concentration has major effect on the practical results of έ and a minor effect on the σ.

Carbon Black does not give dielectric properties by itself. The dielectric properties are generated by space charge polarization at the interface [68]. This phenomenon is known as Maxell-Wanger polarization which explains the dielectric loss ε" due to the polarization that occurs at the interface between the epoxy and CB dispersed at volume fraction below the percolation threshold [68-69].

4.5 Comparison between Theoretical and Practical Results of the Permittivty and Conductivity

The figures below show the comparison between the theoretical results obtained by using Equation 8 and the practical results of the permittivity and conductivity of each CB concentration separately. It is graphically noted that the permittivity and the conductivity curves are diverge as CB concentration is increased

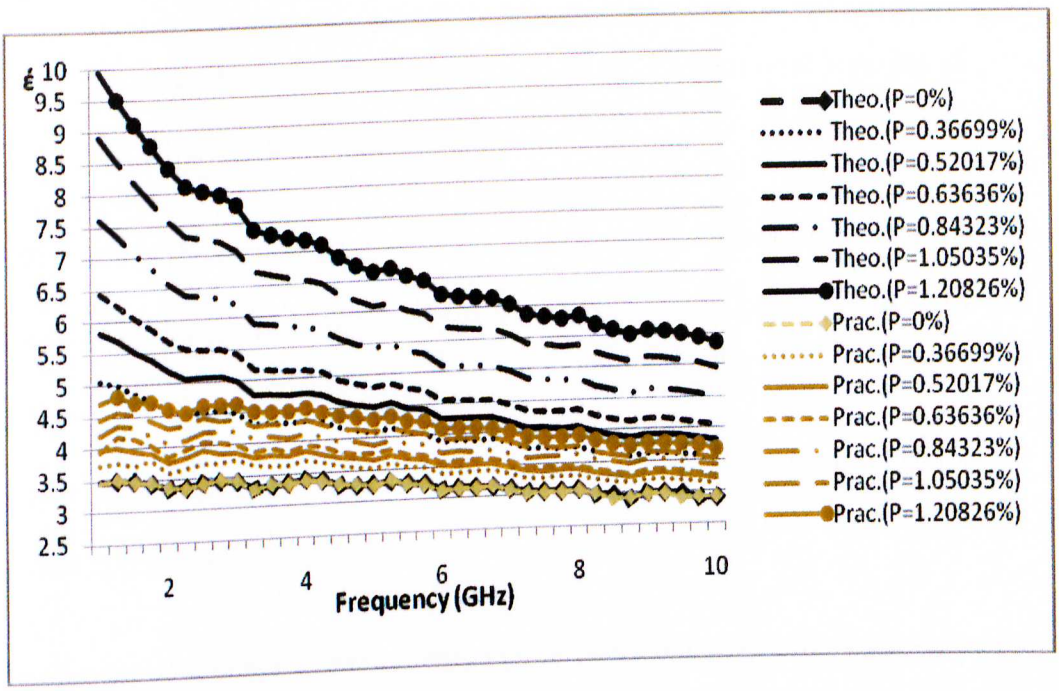

Figure 4.5 Permittivity comparisons between Prac and Theo at the 7 concentration values (levels of concentration "P") and at frequency (1-10) GHz

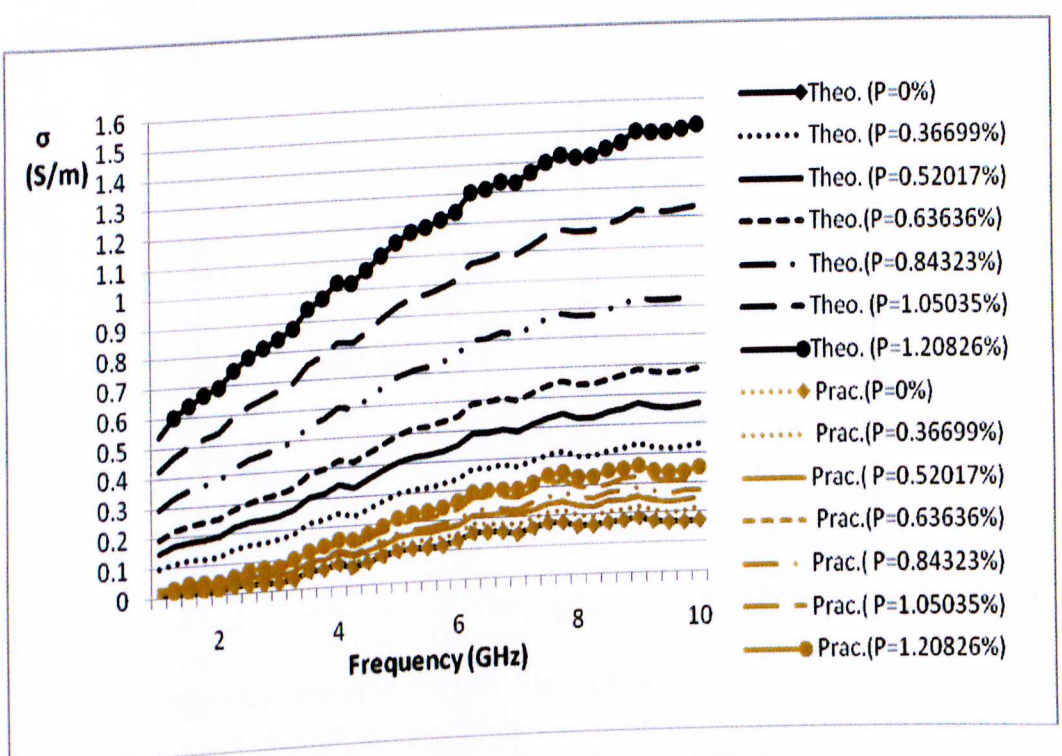

Figure 4.6 Conductivity comparisons between Prac and Theo at the 7 concentration values (levels of concentration "P") and at frequency (1-10) GHz

4.6 Statistical Analysis for the Practical and Theortical Results of Permittivity and Conductivity

Statistical analysis of the permittivity practical- theoretical (Prac-Theo) comparison results at frequency range (1-10) GHz using paired sample t-test are shown in Table 4.10 (P= 0% is not shown since there is an overlapping at this value and it is fully matched). The results show that at all concentration levels there is significant difference since all the p-values are equal to or less than 0.05.

Table 4.10 Permittivity Paired Samples Test of Prac-Theo

Concentration of the comparison between Prac-Theo		Df	Sig. (2-tailed)
Pair 1	0.36699%	5	.005
Pair 2	0.52017%	5	.004
Pair 3	0.63636%	5	.004
Pair 4	0.84323%	5	.004
Pair 5	1.05035%	5	.004
Pair 6	1.20826%	5	.004

Table 4.11 shows the overall analyzing. The p-value is less than 0.05. Hence, Permittivity significantly differs between Prac and Theo based on the descriptive statistics, the mean for Theo is more than the mean for Prac. The graphical presentation is shown in Figure 4.5.

Table 4.11 Permittivity Paired Samples Test of Prac-Theo

	Paired Differences		t	Df	p-value
	Mean	Std. Deviation			
Prac – Theo	-1.476121626119048	1.224143371154093	-7.815	41	.000

Statistical analysis of the conductivity practical- theoretical comparison results at frequency range (1-10) GHz using paired sample test are shown in Table 4.12 (P= 0% is not shown since there is an overlapping at this value and it is fully matched). The results show that at all concentration levels there is a significant diference since all the p-values are less than 0.05.

Table 4.12 Conductivity Paired Samples Test of Prac- Theo

Concentration of the comparison between Prac-Theo		Df	Sig. (2-tailed)
Pair1	0.36699%	5	.001
Pair2	0.52017%	5	.001
Pair 3	0.63636%	5	.001
Pair 4	0.84323%	5	.000
Pair 5	1.05035%	5	.000
Pair 6	1.20826%	5	.000

Table 4.13 shows the overall conductivity comparison of the practical- theoretical results. The p-value is less than 0.05. Hence, Conductivity significantly differs between Prac and Theo based on the descriptive statistics, the mean for Theo being more than the mean for Prac. The graphical presentation is shown in Figure 4.6.

Table 4.13 Conductivity Paired Samples Test of Prac- Theo

	Paired Differences		T	Df	p-value
	Mean	Std. Deviation			
Prac – Theo	-.383087903690476	.320742715345382	-7.740	41	<.0001

4.7 Discussion of the Comparison of the Theoretical and Practical Results of the Permittivty and Conductivity

Figures 4.5 and 4.6 show the comparison between theoretical and practical for έ and σ at each CB concentration. The figures show that the curves do not coincide with each other. However, both curves follow the same trend. At P=0% the curves show that the practical and theoretical curves exactly matched (curves overlapping). This is due to the substitution of P=0 in the equation, which caused the first part (the filler part) in the equation "z p $(\varepsilon^*_1)^k$" to be "zero", therefore, "$(\varepsilon^*)^k$ " will be equal to the epoxy value at the same frequency as follows, $(\varepsilon^*)^k = (\varepsilon^*_2)^k$. Independent Sample t-test, Tables 4.10 and 4.12 showed that there are significant differences between the theoretical curve and practical curve for all the concentration. It is noted that the divergence between the curves increases with the increase of the CB concentration as shown in Figure 4.5 and 4.6. All of these results show that Equation 8 is failed to predict the έ and σ. The used equation was developed numerically from the Lichtenecker-Rother rule; both of epoxy and CB (CB is the same as the one used in this study) should be the same as the ones used to form the equation to ensure accuracy. In this study, the used epoxy had almost the same dielectric properties with the epoxy used by Kim et al [57] to form the equation. A possible reason for

the dielectric properties difference is due to the difference in the vaporizing rate of the used hardener, and that has an effect on the final epoxy volume.

4.8 Comparison between the Modified Equation and the Practical Results of the Permittivity and Conductivity

Since Figure 4.5 and 4.6 clearly show the disagreement between the predication Equation 8 results with the actual measurement results, therefore, a correction factor was introduced to improve the prediction that obtained from the equation. The correction factor was mainly found by try and error. z was divided by (constant value) 3.5 which found to be the best value that minimize the difference between the curves of the practical and the theoretical of the permittivity and the conductivity. The figures below show the comparison between the actual measurements and the values obtained from the modified equation results of permittivity and conductivity. The figures show for each percentage of CB concentration separately.

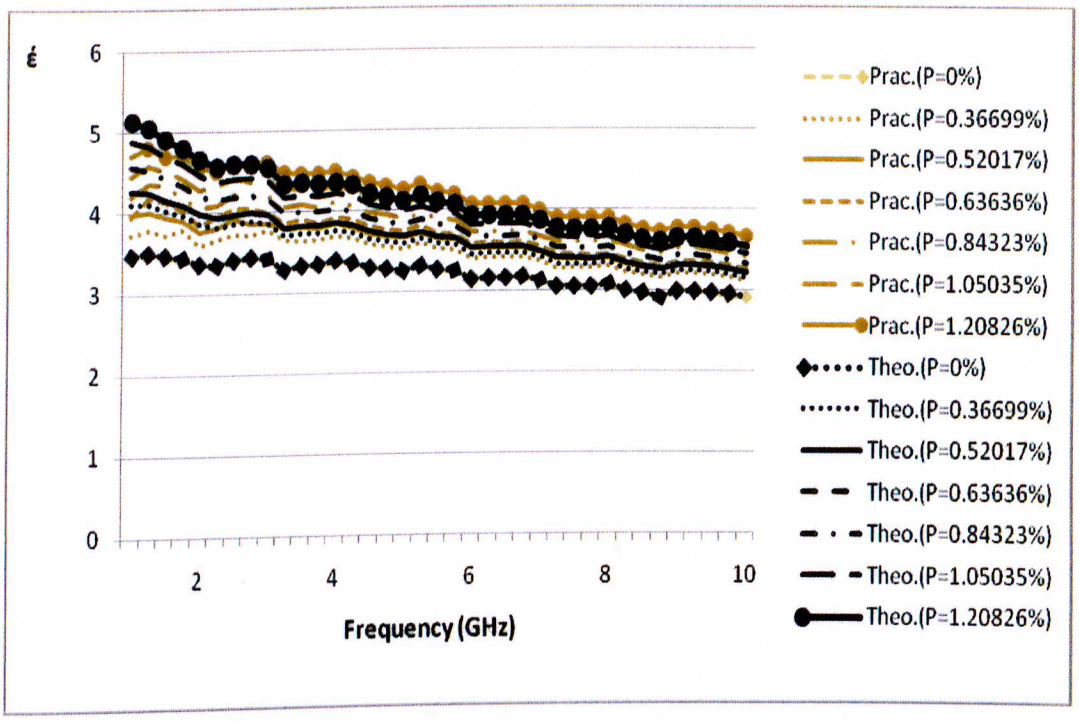

Figure 4.7 Permittivity comparisons between Prac and Theo (after the modification) at the 7 concentration values (levels of concentration "P") and at frequency (1-10) GHz

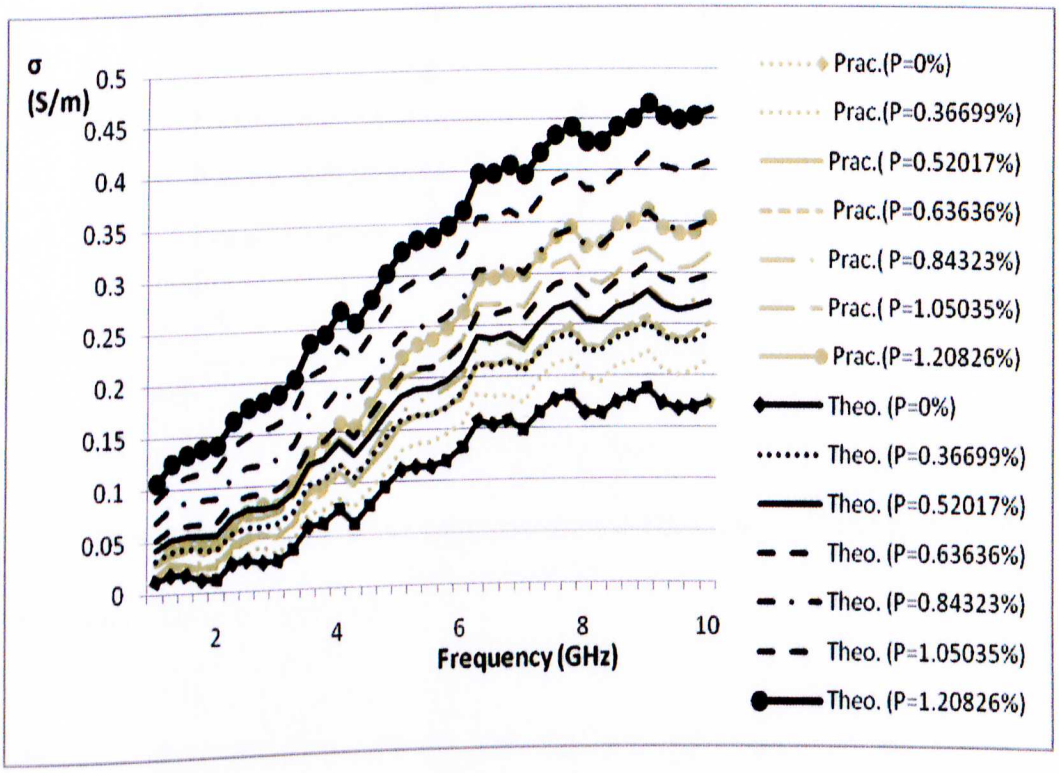

Figure 4.8 conductivity comparisons between Prac and Theo (after the modification) at the 7 concentration values (levels of concentration "P") and at frequency (1-10) GHz

4.9 Statistical Analysis for the Practical and Theoretical (after Modification) Results of Permittivity and Conductivity at Frequency Range (1-10) GHz

Statistical analysis of the permittivity practical- theoretical (after modification) comparison results at frequency range 1 GHz to 10 GHz using paired sample test are shown in Table 4.14 (P = 0% is not shown since there is an overlapping at this value and it is fully matched). The results show that at all concentration levels there are no significant differences since all the p-values is more than 0.05.

Table 4.14 Permittivity Paired Samples Test of Prac-Theo

Concentration of the comparison between Prac-Theo		Df	Sig. (2-tailed)
Pair 1	0.36699%	5	.074
Pair 2	0.52017%	5	.168
Pair 3	0.63636%	5	.536
Pair 4	0.84323%	5	.730
Pair 5	1.05035%	5	.743
Pair 6	1.20826%	5	.934

Table 4.15 shows the overall permittivity comparison. The p-value is more than 0.05. Hence, Permittivity does not differ between Prac and Theo. The graphical presentation of this result is shown in Figure 4.7.

Table 4.15 Permittivity Paired Samples Test of Prac-Theo

	Paired Differences		t	Df	p-value
	Mean	Std. Deviation			
Prac – Theo	-.044734250047619	.163521684572481	-1.773	41	.084

Statistical analysis of the conductivity practical- theoretical comparison results at frequency range 1 GHz to 10 GHz using paired sample test are shown in Table 4.16 (P = 0% is not shown since there is an overlapping at this value and it is fully matched). The results show that at all concentration levels there is a significant difference since all the p-values are less than 0.05.

Table 4.16 Conductivity Paired Samples Test of Prac- Theo

Concentration of the comparesion between Prac-Theo		Df	Sig. (2-tailed)
Pair1	0.36699%	5	.000
Pair2	0.52017%	5	.000
Pair 3	0.63636%	5	.000
Pair 4	0.84323%	5	.000
Pair 5	1.05035%	5	.000
Pair 6	1.20826%	5	.000

Table 4.17 shows the overall conductivity comparison. The p-value is less than 0.05. Hence, conductivity differs between Prac and Theo. The graphical presentation of this result is shown in Figure 4.8.

Table 4.17 Conductivity Paired Samples Test of Prac- Theo

	Paired Differences		t	Df	p-value
	Mean	Std. Deviation			
Prac – Theo	-.049713205833333	.033089248358681	-9.737	41	.000

4.10 Discussion of the Comparison between the Modified Equation and the Practical Results of the Permittivity and Conductivity

Since the equation failed to predict the dielectric properties of the epoxy-CB mixtures, a correction factor to improve the prediction performance was found. Trial and error was used to obtain the correction factor since there was no mathematical base used to develop the equation. Below is the used correction factor.

$$Z=0.922 * f^{0.0416} - 1.8517 \qquad (15)$$

These values have been found to be the best values that balance between the prediction of $\acute{\varepsilon}$ and σ.

Figures 4.7 and 4.8 show the curves comparison between the modified equation results and the practical results of $\acute{\varepsilon}$ and σ. These curves show that the modified equation was successful to predict the $\acute{\varepsilon}$ of epoxy-CB composites, as shown by Independent Sample t-test in Table 4.14 and Figure 4.7. However, the curves for the σ (Figure 4.8) show limited success in σ prediction. The result of Independent Sample t-test in Table 4.16 shows that there is a difference between the practical results and the modified equation results. As the

CAHPTER 5

CONCLUSION & FUTURE WORK

5.1 Conclusion

A method to design phantoms at frequency 1GHz to 10 GHz by using a binary system has been pointed out. A fat phantom model to simulate the electrical properties of the fat tissues could be fabricated using Epoxy – Carbon Black mixture. This mixture could overcome all the problems that the reviewed phantoms suffer from such as: stability over time, hard shaping, complex procedure of making, or no equation for the phantom to adjust the dielectric properties.

Samples of Epoxy-CB with different concentration were manufactured and then tested at frequency range 1GHz to 10GHz by using Network Analyzer.

The prediction equation developed by Kim et al [57]. did not agree with the experimental results and failed to predict the dielectric properties of the epoxy-CB composition in this study. A correction factor was implemented to the equation by J.B. Kim et al. to improve the prediction performance. The changing of the relative dielectric constant with the frequency and the volume concentration of the CB could be well expected by applying the modified equation in frequency range 1 GHz to 10 GHz, while for conductivity it failed to predict the conductivity of the mixture. However, the diverging between the practical and the theoretical results was reduced.

The dielectric properties values were compared to the real fat tissues and the nearest values could be obtained by adjusting the CB concentration to "1.20826%" in frequency range (1-10) GHz.

5.2 Future Work

Future investigation of mixing equations and on the correction factor found in this study is still needed to predict the dielectric properties of Epoxy-CB composites and to possibly maximize the accuracy in designing phantoms.

Additionally, the HWCT phantom study is needed, in order to design tumor and skin models to be used in microwave breast cancer detection application.

REFERENCES

[1] Preece, A. W., Green, J. L., Pothecary, N. and Johnson, R. H. (1994). Microwave Imaging For Tumour Detection. *The Institution of Electrical Engineers, IEE, Savoy Place, London WC2R OBL, UK;* **9**: 1-4.

[2] Nikawa, Y., Chino, M. and Kikuchi, K. (1996). Soft and dry phantom modeling material using silicone rubber with carbon fibre. *IEEE Trans. Microw. Theory Tech;* **44**: 1949-1953.

[3] Ito, K., Furuya, K., Okano, Y. and Hamada, L. (2001). Development and characteristics of a biological tissue-equivalent phantom for microwaves. *Commun. Japan*; **1**: 1126-1135.

[4] Lagendijk, J. J. W. and Nilsson, P. (1985). Hyperthermia dough: a fat and bone equivalent phantom to test microwave/radiofrequency hyperthermia heating systems *Phys. Med. Biol*; **30**: 709-712.

[5] Ibrahim, W. M. A., Algabroun, H. M., Almaqtari, M. T. (2008). Short Review on the Used Recipes to Simulate the Bio-Tissue at Microwave Frequencies. *4th Kuala Lumpur International Conference on Biomedical Engineering 2008, Springer Berlin Heidelberg;* **21**: 234-237.

[6] Neelakanta, S. (2000). Handbook of Electromagnetic Materials. *CRC Press, Inc.*

[7] Larsen, L. E. and Jacobi, J. H. (1979). Microwave scattering parameter imagery of an isolated canine kidney. *Med. Phys*; **6**: 394-403.

[8] Fear, E. C. (2005). Microwave Imaging of the Breast. *Technology in Cancer Research & Treatment;* **4**: 69-82

[9] Fear, E. C., Hagness, S. C., Meaney, P. M., Okoniewski, M. and Stuchly, M. A. (2002). Enhancing Breast Tumor Detection with Near-field Imaging. *IEEE Microwave Mag*; **35** :48-56.

[10] Fear, E. C., Meaney, P. M. and Stuchly, M. A. (2003). Microwaves for Breast Cancer Detection?. *IEEE Potentials*; **22** : 12-18.

[11] Hagness, S. C., Taflove, A. and Bridges, J. E. (1999). Three-dimensional FDTD Analysis of a Pulsed Microwave Confocal System for Breast Cancer Detection: Design of an Antenna-array Element. *IEEE Trans. Ant. Propag*; **47**: 783-791.

[12] Hagness, S. C., Taflove, A. and Bridges, J. E. (1999). Two-dimensional FDTD Analysis of a Pulsed Microwave Confocal System for Breast Cancer Detection: Fixed-focus and Antenna-array sensors. *IEEETrans. Biomed. Eng*; **45**: 1470-1479.

[25] Souvorov, A. E., Bulyshev, A. E, Semenov, S. Y., Svenson, R. H. and G. P. Tatsis. (2000) Two-dimensional Analysis of a Microwave Flat Antenna Array for Breast Cancer Tomography. *IEEE Trans. Microw. Theory. Tech*; **48**: 1413-1415.

[26] Bulyshev, A. E., Semenov, S. Y., Souvorov, A. E., Svenson, R. H., Nazarov, A. G., Sizov Y. E. and Tatsis, G. P. (2001). Computational Modeling of Three-dimensional Microwave Tomography of Breast Cancer. *IEEE Trans. Biomed. Eng;* **48**: 1053-1056.

[27] Hagness, S. C., Taflove, A. and Bridges, J. E. (1998). Two-dimensional FDTD Analysis of a Pulsed Microwave Confocal System for Breast Cancer Detection: Fixed-focus and Antenna-array sensors. *IEEE Trans. Biomed. Eng*; **45**: 1470-1479

[28] Li, X. and Hagness, S. C. (2001). A Confocal Microwave Imaging Algorithm for Breast Cancer Detection. *IEEE Microwave Wireless Components Lett*; **11**: 130-132.

[29] Jayanthy, M., Selvanathan, N., Abu-Bakar, M., Smith, D., Elgabroun, H. M., Yeong, P. M. and Senthil Kumar, S. (2006). Microwave Holographic Imaging Technique for Tumour Detection. *Springer Berlin Heidelberg*;**15**: 275-277.

[30] Elsdon, M., Smith, D., Leach, M. and Foti, S. J. (2006). Experimental investigation of breast tumor imaging using indirect microwave holography. *Microwave and optical technology letters*; **48**: 480-482.

[31] Smith, D., Leach, M. and Sambell, A. J. (2003). Microwave Indirect Holographic Imaging using an Adaptation of Optical Techniques. *IEEE Microwave and Wireless Components Letters*; **13**: 379-381.

[32] Bini, M. G., Ignesti, A., Millanta, L., Olmi, R., Rubino, N. and Vanni, R. (1984). The polyacrylamide as a phantom material for electromagnetic hyperthermia studies. *IEEE Trans. Biomed. Eng;* **31**: 317-322.

[33] Robinson, M. J., Richardson, M. J., Green, J. L. and Preece, A. W. (1991). New materials for dielectric simulation of tissues. *Phys. Med. Biol;* **36**: 1565-71.

[34] Fear, E. C., Hagness, S. C., Paul M. Meaney, Maria A. Stuchly. (2002). Enhancing breast tumor detection with near field imaging, *IEEE Magasine*; **3**:48–56.

[35] Gabriel, C., Gabriel, S. and Corthout, E. (1996). The dielectric properties of biological tissues: I. Literature survey. *Phys. Med. Biol;* **41**: 2231-2249.

[36] Gabriel, S., Lau, R. W. and Gabriel, C. (1996). The dielectric properties of biological tissues: III. Parametric models for the dielectric spectrum of tissues. *Phys. Med. Biol;* **41**: 2271-2293.

[37] Lazebnik, M., McCartney, M., Popovic, D., Watkins, C. B., Lindstrom, M. J., Harter, J., Sewall, S., Magliocco, A., Booske, J. H., Okoniewski, M. and Hagness, S. C. (2007). A large-scale study of the ultrawideband microwave dielectric properties of normal breast tissue btained from reduction surgeries. *Phys. Med. Biol*; **52**: 2637-2656.

[38] Johnson, c. c. and Guy, A. W.(1972). Nonionizing electromagnetic wave effects in biological materials and systems. *Proc. IEEE*; **60**: 692-718.

[39] Guy, W. (1971). Analysis of electromagnetic fields induced in biological tissues by the thermographic studies on equivalent phantom models. *IEEE Trans. Microwave Theory Tech*; **MTT-19**: 205-214.

[40] Chou, C-K., Chen, G-W., Guy, A. W. and Luk, K. H. (1984). Formulas for preparing phantom muscle tissue at various radiofrequencies. B*ioelectromagnetics;* **5**: 435-441.

[41] Kobayashi, T., Nojima, T., Yamada, K. and Uebayashi, S. (1993). Dry phantom composed of ceramics and its application to SAR estimation. *IEEE Trans. Microwave Theory Tech*; **41**: 136-140.

[42] Tamura, H., Ishikawa, Y., Kobayashi, T. and Nojima, T. (1997). A dry phantom material composed of ceramic and graphite powder. *IEEE Trans. Electromagn. Compat*; **39**: 132-137.

[43] Bindu, G., Lonappan, A., Thomas, V., Aanandan, C. k. and Mathew, K. (2006). Dielectric studies of polyvinyl-acetate-based phantom for applications in microwave medical imaging. *Journal of materials science*; **41** : 7419-7424.

[44] Yoshio, N., Masaru, C. and Fumiaki, O. (1992). Study of Dry Phantoms for SAR Simulation. *IEEE*; **1:** 270-271.

[45] Andreuccetti, D., Bini, M. and Ignesti, A. (1988). Use of polyacrylamide as a tissue-equivalent material in the microwave range. *IEEE Trans. Biomed. Eng;* **35**: 275-277.

[46] Meaney, P., Paulsen, K., Hartov, A. and Crane, R. (1996). Microwave imaging for tissue assessment: Initial evaluation in multitarget tissue-equivalent phantoms. *IEEE Trans. Biomed. Eng;* **43**: 878-890.

[47] Surowiec, A., Shrivastava, P. N., Astrahan, M. and Petrovich, Z. (1992). Utilization of a multilayer polyacrylamide phantom for evaluation of hyperthermia applicators. *Int. J. Hyperthermia*; **8**: 795-807.

[48] Davidson, S. R. H. and Sherar, M. D. (2003). Measurement of the thermal conductivity of polyacrylamide tissue-equivalent phantom. *Int. J. Hyperthermia;* **19**: 551-562.

[49] Lazebnik, M., Madsen, E. L., Frank, G. R. and Hagness, S. C. (2005). Tissue-mimicking phantom materials for narrowband and ultrawideband microwave applications. *Phys. Med. Biol;* **50**: 4245-4258.

[50] Li, D., Meaney, P. M. and Paulsen, K. D.(2003). Conformal Microwave Imaging for Breast Cancer Detection. *IEEE Trans. Microw. Theory Tech;* **51**: 1179-1186.

[51] Meaney, P. M., Paulsen, K. D. and Chang, J. T. (1998). Near-field microwave imaging of biologically-based materials using a monopole transceiver system. *IEEE Trans. Microwave Theory Tech;* **46**: 31-45.

[52] Lord Rayleigh (1892). On the influence of obstacles arranged in rectangular order on the properties of a medium. *Phil. Mag.* **34**: 481-502.

[53] Hanai, T.(1960). Theory of the dielectric dispersion due to the interfacial polarization and its applications to emulsion. *Kolloid Z.* **171**: 23–31.

[54] Achour, M. E., Malhi, M. E., Miane, J. L., Carmona, F. and Lahjomri F. (1999). Microwave properties of carbon black–epoxy resin composites and their simulation by means of mixture laws. *J Appl Polym Sci;* **73**: 969-973.

[55] Bottcher, C. J. F. (1973). Theory of Electric Polarization. *Journal of Molecular Structure*; **22** : 155-156.

[56] Neelakantaswamy, P. S., Turkman, R. I. and Sarkar, T. K. (1985). complex permittivity of a dielectric mixture: corrected version of lichtenecker's logarithmic law of mixing. *Electronics Letter*; **21:** 270-271.

[57] Kim, J. B., Kim, T.W. and Kim, C.G. (2006). Simulation method for complex permittivities of carbon black/epoxy composites at microwave frequency band. *J Appl Polym Sci;* **100**: 2189-2195.

[58] Looyenga, H. (1965). Dielectric constant of heterogeneous mixtures. *Physica*; **31**: 401-406.

[59] Stölzle, S., Enders, A. and Nimtz, G. (1992). Numerical simulation of random composite dielectrics. *Journal de Physique I*; **2**: 401-408.

[60] Van Beek, LK. H. (1967). Dielectric behaviour of heterogeneous systems *Progress in Dielectrics*; 7 : 69

[61] Singh, V., Kulkarni, A. R. and Rama Mohan, T. R. (2003). Dielectric properties of aluminum–epoxy composites. *J. Appl. Polym. Sci;* **90**: 3602-3608.

[62] Frohlich, H. (1994). Theory of Dielectrics. *Oxford University Press*

[63] Corkum , R. W. (1952). Isotropic artificial dielectric. *PROC. I.R.E*; **40**; 574-587.

[64] Shin, F. G., Tswi, W. L., Yeung, Y. Y. (1989). Dielectric constant of binary mixtures. *J Mater Sci. Lett;* **8**: 1383-1385

[65] Measurement of Dielectric Material Properties (Rohde - Schwarz) http://www2.rohde-schwarz.com/file_3463/RAC-0607-0019.pdf

[66] Microwave Dielectric Spectroscopy Workshop (Agilent) http://www.home.agilent.com/upload/cmc_upload/All/MWDielectricSpectroscopyWS.pdf

[67] Basics of Measuring the Dielectric Properties of Materials (Agilent) http://www3.imperial.ac.uk/pls/portallive/docs/1/11949698.PDF

[68] Moon, K. S., Choi, H. D., Lee, A. K., Cho, K. Y., Yoon, H. G. and Suh, K. S. (2000). Dielectric properties of epoxy-dielectrics-carbon black composite for phantom materials at radio frequencies. *J Appl Polym Sci;* **77** : 1294-1302.

[69] Barba, A. A., Lamberti, G., D'Amore, M. and Acierno, D. (2006). Carbon Black/Silicone Rubber Blends as Absorbing Materials to Reduce Electro Magnetic Interferences (EMI). *Polymer Bulletin*; **57**: 587-593.

APPENDIX

Table Dunnett T3 Multiple Comparisons

(I) Concentration	(J) Concentration	Mean Difference (I-J)	Std. Error	Sig.
0%	0.36699%	-.176978066500000	.064069340134909	.283
	0.52017%	-.275880791166667	.076764600391130	.114
	0.63636%	-.275880791166667	.076764600391130	.114
	0.84323%	-.545600633000000*	.110613731885875	.035
	1.05035%	-.770750743500000*	.137930549993386	.022
	1.20826%	-.974901807000000*	.162111520761750	.017
0.36699%	0%	.176978066500000	.064069340134909	.283
	0.52017%	-.098902724666667	.090802042688722	.991
	0.63636%	-.098902724666667	.090802042688722	.991
	0.84323%	-.368622566500000	.120779156997202	.197
	1.05035%	-.593772677000000	.146208904327720	.066
	1.20826%	-.797923740500000*	.169210969641219	.037
0.52017%	0%	.275880791166667	.076764600391130	.114

	0.36699%	.098902724666667	.090802042688722	.991
	0.63636%	.000000000000000	.100164537059439	1.000
	0.84323%	-.269719841833333	.127966903114993	.576
	1.05035%	-.494869952333333	.152200417977743	.154
	1.20826%	-.699021015833333	.174414092821678	.068
0.63636%	0%	.275880791166667	.076764600391130	.114
	0.36699%	.098902724666667	.090802042688722	.991
	0.52017%	.000000000000000	.100164537059439	1.000
	0.84323%	-.269719841833333	.127966903114993	.576
	1.05035%	-.494869952333333	.152200417977743	.154
	1.20826%	-.699021015833333	.174414092821678	.068
0.84323%	0%	.545600633000000*	.110613731885875	.035
	0.36699%	.368622566500000	.120779156997202	.197
	0.52017%	.269719841833333	.127966903114993	.576
	0.63636%	.269719841833333	.127966903114993	.576
	1.05035%	-.225150110500000	.171777650004621	.960
	1.20826%	-.429301174000000	.191736458670017	.502

1.05035%	0%	.770750743500000*	.137930549993386	.022
	0.36699%	.593772677000000	.146208904327720	.066
	0.52017%	.494869952333333	.152200417977743	.154
	0.63636%	.494869952333333	.152200417977743	.154
	0.84323%	.225150110500000	.171777650004621	.960
	1.20826%	-.204151063500000	.208691898556405	.997
1.20826%	0%	.974901807000000*	.162111520761750	.017
	0.36699%	.797923740500000*	.169210969641219	.037
	0.52017%	.699021015833333	.174414092821678	.068
	0.63636%	.699021015833333	.174414092821678	.068
	0.84323%	.429301174000000	.191736458670017	.502
	1.05035%	.204151063500000	.208691898556405	.997